Two-stage mid-Brunhes climate transition and mid-Pleistocene human diversification

Ao Hong [1, 2, 3, 4, *], Rohling Eelco J. [5, 6], Stringer Chris [7], Roberts Andrew P. [5], Dekkers Mark J. [8], Dupont-Nivet Guillaume [9], Yu Jimin [5], Liu Qingsong [10], Zhang Peng [1, 3], Liu Zhonghui [11], Ma Xiaolin [1, 3], Zhou Weijian [1, 2, 3], Jin Zhangdong [1, 2, 3, 12], Xiao Guoqiao [4], Wang Hong [13], Sun Qiang [14], Yang Pingguo [15], Peng Xianzhe [4], Shi Zhengguo [1], Qiang Xiaoke [1], An Zhisheng [1, 2, 3]

[1] State Key Laboratory of Loess and Quaternary Geology, Institute of Earth Environment, Chinese Academy of Sciences, Xi'an, China
[2] CAS Center for Excellence in Quaternary Science and Global Change, Chinese Academy of Sciences, Xi'an, China
[3] Open Studio for Oceanic-Continental Climate and Environment Changes, Pilot National Laboratory for Marine Science and Technology (Qingdao), Qingdao, China
[4] State Key Laboratory of Biogeology and Environmental Geology, School of Earth Sciences, China University of Geosciences, Wuhan, China
[5] Research School of Earth Sciences, Australian National University, Canberra, Australia
[6] Ocean and Earth Science, University of Southampton, National Oceanography Centre, Southampton, UK
[7] Centre for Human Evolution Research (CHER), Department of Earth Sciences, Natural History Museum, London, UK
[8] Paleomagnetic Laboratory 'Fort Hoofddijk', Department of Earth Sciences, Faculty of Geosciences, Utrecht University, Utrecht, the Netherlands
[9] Université de Rennes, CNRS, Géosciences Rennes, Rennes, France
[10] Centre for Marine Magnetism (CM2), Department of Ocean Science and Engineering, Southern University of Science and Technology, Shenzhen, China
[11] Department of Earth Sciences, University of Hong Kong, Hong Kong, China
[12] Institute of Global Environmental Change, Xi'an Jiaotong University, Xi'an, China
[13] Interdisciplinary Research Center of Earth Science Frontier, Beijing Normal University, Beijing, China
[14] College of Geology and Environment, Xi'an University of Science and Technology, Xi'an, China
[15] College of Life Sciences, Shanxi Normal University, Linfen, China

* Corresponding author : Hong Ao, email address : aohong@ieecas.cn

Abstract :

Global climate shifted to markedly warmer interglacial conditions across the "mid-Brunhes transition" (MBT, ~400 ka). However, a global MBT synthesis that spans marine and terrestrial evidence remains elusive, which limits our understanding of the role of the MBT in mid-Pleistocene human evolution. We synthesize Asian precipitation reconstructions within a context of global palaeoclimatic records and find that the MBT occurred in two stages. First, stronger warming of northern hemisphere continents, weaker southern hemisphere warming, and related more extensive northward displacement of the intertropical convergence zone (ITCZ) during interglacial marine isotope stage (MIS) 13 intensified and expanded precipitation in Asian monsoon regions and in other widespread northern hemisphere regions, with

accompanying carbon reservoir changes featuring globally high marine benthic δ13C values because of vegetation expansion at ~500 ka. Subdued southern hemisphere warming and northward ITCZ displacement decreased southern hemisphere precipitation simultaneously during MIS 13. Second, a shift to globally warmer interglacials at ~400 ka, with elevated atmospheric CO2 concentrations, smaller ice volume, and higher sea level resulted in sustained high interglacial precipitation in East Asia from MIS 11 onward and sustained high marine benthic δ13C values during MIS 11. We also synthesize palaeoanthropological data and find that the climate and ecosystem changes across the MBT coincided with the timing of human lineage diversification, including the emergence of Neanderthals and Denisovans in Eurasia and Homo sapiens in Africa, and their potential coexistence with H. heidelbergensis, H. erectus, H. floresiensis, H. naledi, and other Homo archaics. The timing of the MBT also coincided with novel hominin behavioural developments, including fire control and the transition from handaxe industries to more versatile Levallois techniques. Combined with environmental theories of human evolution, this chronological coincidence suggests a potential link between mid-Pleistocene environmental and human evolution.

1. Introduction

Marine benthic $\delta^{18}O$, deep-sea temperature, and Antarctic ice core temperature records suggest a notable transition from "lukewarm" to warmer "super" interglacials during the middle Brunhes geomagnetic polarity chron, starting with interglacial marine isotope stage (MIS) 11 (Augustin et al., 2004; Lisiecki and Raymo, 2005; Jouzel et al., 2007; Lang and Wolff, 2011; Elderfield et al., 2012; Hodell et al., 2013; Berger et al., 2016). This transition has become known as the mid-Brunhes transition (MBT) or mid-Brunhes event (MBE) (e.g., Jansen et al., 1986; Candy et al., 2010; Blain et al., 2012; Hodell et al., 2013; Yin, 2013; Wang et al., 2014). Climate variations across the MBT provide a backdrop to mid-Pleistocene human evolution and dispersal, including the origination of Neanderthals in western Eurasia, Denisovans in eastern Eurasia, and *Homo sapiens* in Africa, the transition from flake- and handaxe-dominated assemblages to the more versatile Levallois technique, and permanent habitation of many high-latitude Eurasian regions by *H. heidelbergensis* and/or other *Homo* archaics with handaxe and/or Levallois technologies (Rightmire, 1998; Hublin, 2009; Stringer, 2012a, b; Hublin et al., 2017; Richter et al., 2017; Owen et al., 2018; Potts et al., 2018).

Environmental theories of human evolution suggest that key evolutionary changes were mediated by shifts in climate and ecosystem variability (e.g., deMenocal, 1995, 2004; Potts, 1996; Potts et al., 2018). However, how orbitally-induced climate and habitat changes across the MBT may have

impacted mid-Pleistocene human evolution, adaptive context, dispersal, and technological development remains largely unexplored (Hublin, 2009; Owen et al., 2018; Potts et al., 2018). East Asia is a critical region for these developments. For example, the earliest human occupation of the Chinese Loess Plateau, central China, is dated to ~2.1 Ma (Zhu et al., 2018), which is similar to a claimed first *H. erectus* appearance in southern Africa at ~2 Ma (Herries et al., 2020). Abundant Palaeolithic sites spanning the early and middle Pleistocene have been found in East Asia, many with accompanying *H. erectus* or other *Homo* archaic fossils (An and Ho, 1989; Zhu et al., 2001, 2003, 2004, 2008, 2015, 2018; Dennell, 2009; Ao et al., 2013a, 2013b, 2017).

We here reconstruct terrestrial Asian summer monsoon precipitation (hydroclimate) changes over the past 800 kyr using new high-resolution environmental magnetic records from a loess section on the Chinese Loess Plateau and existing wider regional records. We then consider these Asian monsoonal records within a global context of worldwide hydroclimate records, marine sediment records, and Antarctic ice-core records to evaluate Asian monsoon dynamics in relation to global climate changes across the MBT. Finally, we synthesize mid-Pleistocene palaeoclimatic and palaeoanthropological records to infer potential human evolutionary responses associated with marked global and regional climate shifts across the MBT.

2. Mid-Brunhes Asian summer monsoon transition on the Chinese Loess Plateau

Like monsoonal Africa, the Chinese Loess Plateau climate is dominated by seasonally alternating summer and winter monsoon changes (Figs. 1 and 2). Warm/humid southeasterly summer monsoon penetration inland from tropical oceans produces rains from May to September that contribute 60–75% of annual precipitation. In contrast, the northwesterly winter monsoon transports high-latitude cold

and dry air masses and dust from arid regions located to the west and north to the downwind Chinese

Loess Plateau (Guo et al., 2009; Hao et al., 2012; Sun et al., 2020). With thicknesses of up to ~600 m,

aeolian dust accumulations on the Chinese Loess Plateau provide a unique high-resolution archive of

climate variations from the latest Oligocene through the Quaternary (Guo et al., 2002; Qiang et al.,

2011; An, 2014; Sun et al., 2020). High Quaternary summer monsoon precipitation during

interglacials drove accelerated pedogenesis and *in situ* red soil development within yellow loess, while

strong winter monsoons during glacials with substantially weakened summer monsoon intensity

resulted in deposition of insignificantly altered loess (An et al., 1990; Guo et al., 2009; Hao et al.,

2012; Maher, 2016). Therefore, well-developed Quaternary loess-palaeosol sequences on the Chinese

Loess Plateau preserve an outstanding terrestrial archive of past climate changes linked to both high-

and low-latitude processes (Guo et al., 2009; Hao et al., 2012; An, 2014; Sun et al., 2020).

Stronger *in situ* pedogenesis during periods of increased precipitation accelerates formation of

fine magnetite/maghemite, the concentration of which can be measured by low-frequency magnetic

susceptibility (χ_{lf}) or frequency-dependent magnetic susceptibility (χ_{fd}) (Zhou et al., 1990; Maher and

Thompson, 1995; Maher, 1998, 2016). Stronger pedogenesis also results in formation of more

hematite (Hm) than goethite (Gt), which translates to higher Hm/Gt ratios (Torrent et al., 2007). This

is consistent with the red colour of palaeosol layers, which imprint significantly the red colour of

hematite. Thus, loess χ_{lf}, χ_{fd}, and Hm/Gt are considered to be meaningful proxies for summer monsoon

precipitation (e.g., An et al., 1990; Maher and Thompson, 1995; Torrent et al., 2007; Guo et al., 2009;

Hao et al., 2012; Maher, 2016).

To reveal orbital-scale variability in summer monsoon precipitation during the last 800 kyr, χ_{lf}

and Hm/Gt were measured for 3,264 samples from the Binxian loess section (35°2′N, 108°5′E) on the

central Chinese Loess Plateau (Fig. 2). Measurements were made at 2-cm stratigraphic intervals (for details see Supplementary Methods), i.e. with a high temporal resolution of ~0.3 kyr, which exceeds that of most mid-Pleistocene loess palaeoclimate records. Comparison with previous records, notably the Xifeng loess χ_{lf} time series (Guo et al., 2009), reveals consistent χ_{lf} variability across the Chinese Loess Plateau (Fig. 3), which allows synchronization of records over glacial-interglacial time scales. Even before synchronization, major glacial-interglacial cycles are clearly evident in the different χ_{lf} records (Fig. 3), which were formulated with different approaches. All approaches identify similar chronologies for the sequence of palaeosol layers S_0 to S_7 over the last 800 kyr, and the same correlations of loess and palaeosol layers to glacial and interglacial periods defined by the marine benthic $\delta^{18}O$ record (Lisiecki and Raymo, 2005) (Fig. 3). Chronological uncertainties do not result in major differences in loess-to-marine correlations across 100-kyr glacial-interglacial cycles (Fig. 3). Our age model was established by χ_{lf} correlation between the Binxian and Xifeng sections using 24 age correlation points that have the same χ_{lf} features (black dots in Fig. 3). Synchronization with the Xifeng loess χ_{lf} time series, which is based on a pedostratigraphic loess-to-marine correlation (Guo et al., 2009), results in a relatively higher correlation coefficient (R = 0.8) between the Binxian χ_{lf} and marine benthic $\delta^{18}O$ records than synchronization with other loess time scales.

Temporal χ_{lf} variability in the Binxian section over the last 800 kyr matches not only that in other sections across the Chinese Loess Plateau, but also glacial-interglacial cycles in the marine benthic $\delta^{18}O$ record (Lisiecki and Raymo, 2005) (Fig. 4). Throughout, elevated summer monsoon precipitation caused formation of interglacial red palaeosol layers, which have higher χ_{lf} and Hm/Gt values than glacial yellow loess layers that accumulated under strong winter monsoon and weak summer monsoon conditions (Figs. 4 and 5). Within this general interglacial-glacial pattern, palaeosol

7

layers S_{5-1}, S_4, S_3, S_2, S_1, and S_0 ($\leq$ 500 ka) are more strongly developed with higher χ_{lf} and Hm/Gt

values than palaeosol layers S_7, S_6, S_{5-3}, and S_{5-2} that are older than 500 ka (Figs. 4 and 5). The

interglacial amplitude increase across the MBT is larger in the χ_{lf} record than in the Hm/Gt record (Fig.

5 A, B), which is likely due to different proxy sensitivities to monsoon changes. Regardless, both the

χ_{lf} and Hm/Gt records indicate that MIS 13 was the first interglacial with enhanced pedogenesis and

increased summer monsoon precipitation on the Chinese Loess Plateau. This is consistent with

previous inferences from increased ratios between pedogenic free Fe_2O_3 and total Fe_2O_3 (a measure of

iron liberated by chemical weathering; Guo et al. (2009)), redness (a measure of pedogenic

development; Guo et al. (2009)), χ_{lf}, and χ_{fd} for other loess sections across the wider Chinese Loess

Plateau (Hao et al., 2012; Zhang et al., 2016) (Fig. 4A, B).

3. Two-stage mid-Brunhes climate transition

3.1. Strong interhemispheric contrasts during MIS 13 and onset of super-interglacials at MIS 11

The observed transition to higher precipitation on the Chinese Loess Plateau coincided with a

positive marine benthic $\delta^{13}C$ shift in MIS 13, but predated by ~100 kyr shifts during MIS 11 in the

records of marine benthic $\delta^{18}O$, ice volume, sea level, and atmospheric CO_2 concentration records

(Wang et al. 2003; Augustin et al., 2004; Lisiecki and Raymo, 2005; Lüthi et al., 2008; Elderfield et

al., 2012; Martínez-Botí et al., 2015; Spratt and Lisiecki, 2016) (Fig. 5). To assess Asian summer

monsoon changes and dynamics across the MBT in a global perspective, we compare Chinese Loess

Plateau records with globally more widespread precipitation and temperature records (Figs. 1 and 5–7;

Tables 1–2).

Global datasets that indicate precipitation changes across the MBT are summarized in Table 1.

8

Similar to the MIS 13 shift to higher precipitation on the Chinese Loess Plateau, such a shift is also evident in other regions of Asia, North Africa, Europe, the Middle East, northernmost South America, and the equatorial Pacific Ocean (Table 1; Fig. 1). For example, the *Artemisia*/Chenopodiaceae ratio increased during MIS 13 and especially during MIS 11 in the Yinchuan Basin, NW China, which is consistent with higher precipitation (Li et al., 2017a). Terrestrial sedimentary, soil micromorphological, mineralogical, and geochemical records from South China (Zhang et al., 2009; Lu et al., 2020) and marine geochemical records (e.g., *n*-alkane flux, sea-surface salinity, foraminiferal $\delta^{15}N$, and opal content) from the South China Sea (Chyu et al., 2001; Shiau et al., 2008; Li et al., 2013; Ren et al., 2017) also suggest a precipitation increase during MIS 13 relative to previous interglacials. Higher South Asian monsoon intensity has been inferred from MIS 13 onward from higher Arabian Sea productivity as indicated by enhanced Ca/K ratios (Kunkelova et al., 2018) (Fig. 5C) and Ba concentrations (Ziegler et al., 2010) (Fig. 6A), and from larger lithogenic grain sizes that reflect stronger detrital transportation by summer monsoon precipitation (Clemens et al., 1996).

In North Africa, increased monsoon precipitation enhanced discharge into the Mediterranean Sea from rivers along the North African margin, including the Nile, which caused formation of a thick sapropel in Eastern Mediterranean sediments during MIS 13, with low Si/Al and K/Al ratios (Rossignol-Strick et al., 1998; Zhao et al., 2012). Further support for a shift to higher North African precipitation comes from the clay mineralogy of Nile deep-sea fan sediments (Zhao et al., 2012) (Fig. 5D) and from the emergence of large ephemeral lakes in the present-day Sahara Desert (Geyh and Thiedig, 2008). Widespread formation of a well-developed palaeosol layer (S5) in the Danube River basin and increases in *Pinus* pollen and total organic carbon (TOC) contents and Ca/K from Lake Van, Turkey, suggest increased precipitation during MIS 13 in Europe and the Middle East, respectively

(Litt et al., 2014; Stockhecke et al., 2014; Marković et al., 2015).

In northernmost South America (northern Colombia), lake records indicate that MIS 13 became prominently warmer and wetter than MIS 15 as suggested by decreased shallow water taxa and increased *Alnus*, arboreal, and aquatic cyperaceae pollen (Hooghiemstra and Ran, 1994; Torres et al., 2013). Likewise, a shift to higher precipitation at MIS 13 enhanced regional vegetation cover that stabilized landscapes, which would have reduced terrigenous input into the western tropical Atlantic Ocean and easternmost equatorial Pacific Ocean from northern South America (Harris et al., 1997; Horikawa et al., 2010). Relatively high $CaCO_3$ (Fig. 5E) and longer-chain *n*-alkanes concentrations are thus observed during MIS 13 in the western tropical Atlantic and easternmost equatorial Pacific Oceans, respectively (Harris et al., 1997; Horikawa et al., 2010). In addition, a shift to increased interglacial precipitation in the Pacific Ocean at MIS 13 is indicated by more negative shifts in surface-dwelling *Globigerinoides ruber* $\delta^{18}O$ and seawater $\delta^{18}O$ records at ODP Hole 806B (Medina-Elizalde and Lea, 2005), and increased biogenic opal flux in core PC72 (Murray et al., 2012) (Fig. 6B–D).

In contrast to a change to wetter conditions in widespread regions across the northern hemisphere, the climate became drier from MIS 15 to 13 in South Africa and South Australia. In subtropical southeastern Africa, decreased Fe/Ca ratios (Fig. 5F) in marine sediments offshore of the Limpopo River mouth, increased grassland pollen and decreased aquatic pollen in Lake Magadi, and shallowing or even the disappearance of some lakes in South Africa indicate a shift to drier conditions in MIS 13 (Ivory et al., 2016; Caley et al., 2018; Owen et al., 2018). Likewise, South Australia became drier as suggested by transitions from freshwater lacustrine to aeolian and saline gypsiferous deposits in the Lefroy and Bungunnia lakes at ~500 ka (An et al., 1986; Zheng et al., 1998).

Global datasets that indicate temperature changes across the MBT are summarized in Table 2. Like precipitation, temperature appears to have changed asymmetrically between hemispheres during MIS 13 (Guo et al., 2009) (Fig. 1). Sub-Antarctic Pacific Ocean deep-sea temperature (Elderfield et al., 2012) (Fig. 5J), Antarctic atmospheric temperature (Jouzel et al., 2007), South Atlantic and South Indian Ocean sea surface temperature (SST) (Etourneau et al., 2009; Martínez-Garcia et al., 2009), and stacked Southern Ocean SST all indicate that MIS 13 was the coolest among the last nine interglacials (Fig. 7A–E). Moreover, increased sea-salt sodium fluxes in the Dome C ice core suggest increased interglacial sea ice volume around Antarctica during MIS 13 (Wolff et al., 2010) (Fig. 7F). Ice sheet modelling (Pollard and Deconto, 2009) indicates an ice volume increase in Antarctica from MIS 15 to 13 (Fig. 7G). Southern Ocean Ba/Fe and Ca/Fe records generally have prominent peaks during interglacials, but they have a muted peak during MIS 13, which suggests substantially lower export production linked to a regionally cooler climate (Jaccard et al., 2013).

In contrast to subdued southern hemisphere warming, northern hemisphere continents became notably warmer from MIS 15 to 13 (Fig. 1). Sharp increases in manganese, spermatophyte pollen, and pteridophyte spores in Arctic marine sediments (de Vernal and Hillaire-Marcel, 2008; Polyak et al., 2013) suggest a significantly warmer Arctic climate during MIS 13 than MIS 15 (Fig. 7H–J). In Lake El'gygytgyn (NE Russia), Mn/Fe and diatom concentration increased during MIS 13 and more significantly during MIS 11, which suggests elevated interglacial temperatures (Melles et al., 2012; Snyder et al., 2013) (Fig. 7K–L). Widespread and unusually warm MIS 13 conditions are also suggested by temperature reconstructions and pollen data from New Mexico (Fawcett et al., 2011; Contreras et al., 2016), palaeoecological records from Britain (Candy and McClymont, 2013), pollen data from Tenaghi Phillipon, Greece (Pross et al., 2015), terrestrial and marine pollen data from Italy

(Combourieu-Nebout et al., 2015; Margari et al., 2018), planktonic diatom assemblages from Lake Baikal, central Asia (Prokopenko et al., 2002), and lake carbonate and pollen records from the eastern Tibetan Plateau (Chen et al., 1999). Modern mammalian fauna and vegetation were also established in southern Europe at ~0.5 Ma, which is consistent with establishment of modern warm interglacials (Magri and Palombo, 2013).

The above observations (Figs. 1 and 5–7; Tables 1–2) indicate asymmetrical changes between hemispheres in both precipitation and temperature across MIS 13, as noted by Guo et al. (2009). This suggests that the Chinese Loess Plateau precipitation increase during MIS 13 was related to a global mechanism rather than to regional factors only. Intense northern hemisphere warming tends to increase water vapour formation above the northern oceans and to enhance atmospheric ascent (Beck et al., 2018), which may have driven the widespread precipitation increase on the Chinese Loess Plateau and in other northern hemisphere regions during MIS 13, including Eurasia, North Africa, northernmost South America, and the equatorial Pacific Ocean (Fig. 1 and Table 1). In contrast, lower southern hemisphere temperatures promoted decreased precipitation in South Africa and Australia during MIS 13. In the same period, more intense northern hemisphere warming together with subdued southern hemisphere warming, possibly due to stronger obliquity-induced summer insolation in northern compared to southern hemisphere continents (Yin and Berger, 2012; Berger et al., 2016), may have resulted in intensification and more extensive northward swings of the intertropical convergence zone (ITCZ) relative to previous interglacials. This ITCZ displacement also facilitated a precipitation increase over Asia, North Africa, northernmost South America, and the equatorial Pacific Ocean, but resulted in precipitation decreases in South Africa and South Australia (An, 2000; Chiang and Bitz, 2005; Guo et al., 2009; An et al., 2011; Schneider et al., 2014; Shi et al., 2020) (Fig.

1). Recent climate model simulations provide crucial support for such responses during hemispherically asymmetric MIS 13 climate changes (Shi et al., 2020).

After MIS 13, all interglacials were characterized by sustained high interglacial precipitation in East Asia. However, the marked hemispheric asymmetry typical of MIS 13 is absent in the later interglacials. Hence, the dynamics underpinning high monsoon intensity (and precipitation) from MIS 11 onward require a separate explanation. Starting with MIS 11, interglacials transitioned from so-called "lukewarm" to warmer "super" interglacials, with reduced global ice volume (and, thus, higher sea level), and with elevated atmospheric CO_2 concentrations (Augustin et al., 2004; Lisiecki and Raymo, 2005; Lüthi et al., 2008; Elderfield et al., 2012; Martínez-Botí et al., 2015; Spratt and Lisiecki, 2016) (Fig. 5). Carbon-cycle and ice-albedo feedbacks likely played critical roles in intensifying and sustaining interglacial warming, based on both model simulations and observed higher interglacial CO_2 concentrations during MIS 11 and younger interglacials, with synchronous sea level increases (Lisiecki and Raymo, 2005, Rohling et al., 2009, 2014; Tzedakis et al., 2009; Yin and Berger, 2010; Lang and Wolff, 2011; Grant et al., 2014; Spratt and Lisiecki, 2016). These globally increased interglacial intensities were associated with increased lower-tropospheric water vapour loading in the Western Pacific and Indian Oceans, strengthened summer monsoon circulation, and shortened moisture transportation pathways to East Asia. Combined, they would have enhanced moisture transportation to East Asia (Ao et al., 2012; Beck et al., 2018) to lead to sustained high interglacial precipitation.

3.2. Oceanic carbon cycle changes and a two-stage climate transition across the MBT

High interglacial marine benthic $\delta^{13}C$ values during MIS 11 are consistent with the parallel low

marine benthic $\delta^{18}O$ values, high atmospheric CO_2 concentrations, low ice volume, and high sea level (Figs. 5 and 8). However, earlier high interglacial marine benthic $\delta^{13}C$ values during MIS 13 are incompatible with the notably higher marine benthic $\delta^{18}O$ values, lower atmospheric CO_2 concentrations, higher ice volume, and lower sea level, relative to MIS 11 (Figs. 5 and 8). Ocean carbon chemistry and deep-water circulation changes have often been used to explain abnormally high benthic $\delta^{13}C$ values during MIS 13 (Raymo et al., 1997; Wang et al., 2003; Hoogakker et al., 2006; Holden et al., 2011). Although benthic $\delta^{13}C$ can be influenced by ocean circulation changes, the fact that this positive $\delta^{13}C$ shift is observed so widely in the global ocean, including the South China Sea (Wang et al., 2003, 2014), tropical eastern Pacific Ocean (Mix et al., 1995), North Atlantic Ocean (Tiedemann et al., 1994), South Pacific Ocean (Elderfield et al., 2012), and Southern Ocean (Venz and Hodell, 2002), as is evident from the global benthic $\delta^{13}C$ stack (Fig. 8), reflect global carbon reservoir changes at MIS 13 (Wang et al., 2003). A growing number of studies (e.g., Gingele and Schmieder, 2001; Lear et al., 2016; Howe and Piotrowski, 2017; Sosdian et al., 2018; Farmer et al., 2019) provide evidence that deep-water circulation was not anomalous, so that it was not responsible for the prominent benthic $\delta^{13}C$ shift at MIS 13. For example, seawater ε_{Nd} (Fig. 9A) in the equatorial western Atlantic Ocean (Howe and Piotrowski, 2017), benthic foraminiferal trace element B/Ca (Fig. 9B), Cd/Ca, and planktonic foraminiferal U/Ca in the North Atlantic Ocean (Lear et al., 2016; Sosdian et al., 2018; Farmer et al., 2019), and kaolinite/chlorite ratios (Fig. 9C) in the South Atlantic Ocean (Gingele and Schmieder, 2001) all suggest that MIS 13 deep-water circulation was not different from other interglacials. Thus, we view the positive MIS 13 benthic $\delta^{13}C$ shift to be due to global carbon reservoir changes, as originally suggested by Wang et al. (2003). Wang et al. (2014) suggested that the MIS 13 benthic $\delta^{13}C$ shift may be (partly) attributed to potential Southern Ocean changes, via changes

in the ratio of oceanic particulate to dissolved organic carbon. However, based on concurrent and widespread increases in precipitation and forest/vegetation cover over northern hemisphere continents (Fig. 1 and Table 1), we suggest that increased ^{12}C sequestration into continental (and continental shelf) biomass likely dominated the increase in dissolved inorganic carbon $\delta^{13}C$ that is recorded in marine benthic foraminifera.

Our synthesis of global middle to late Pleistocene palaeoclimate and benthic $\delta^{13}C$ records indicates that markedly asymmetrical inter-hemispheric temperature and precipitation changes, prominent northward ITCZ swings, and profound global carbon cycle changes occurred as early as MIS 13 (Fig. 5). In contrast, atmospheric CO_2 concentrations, global mean annual surface air temperature, South Atlantic Ocean deep-sea temperature, global sea level, and global benthic $\delta^{18}O$ went through a major transition as late as MIS 11 (Lisiecki and Raymo, 2005; Lüthi et al., 2008; Elderfield et al., 2012; Martínez-Botí et al., 2015; Spratt and Lisiecki, 2016) (Fig. 5). Hence, we conclude that the mid-Brunhes climate transition occurred in two stages. The first stage (MBT-1) was marked by asymmetrical temperature and precipitation changes between hemispheres, northward ITCZ displacement, and global carbon cycle changes during MIS 13. The second stage (MBT-2) was marked by global "mean" climate changes in atmospheric CO_2 concentrations, global atmospheric and deep-sea temperatures, and ice volume/sea level during MIS 11 (Fig. 5). Both the Greenland and West Antarctic ice sheets may have collapsed during the warm "super" interglacial MIS 11 (Raymo and Mitrovica, 2012; Reyes et al., 2014).

Our proposed two-stage MBT development reconciles different MBT timings from palaeoclimate records (Fig. 5). Some regions responded predominantly to northern hemisphere continental warming and northward ITCZ displacement during MBT-1, such as mid- and low-latitude

15

Asian and North African precipitation, which featured maximum values during MIS 13. This induced

intense palaeosol development on the Chinese Loess Plateau (Fig. 4) and formation of a thick Eastern

Mediterranean sapropel (e.g., Rossignol-Strick et al., 1998). Some other regions, such as the Yinchuan

Basin (NW China) and high-latitude NE Russia, responded only moderately to northern hemisphere

continental warming and to a northward ITCZ displacement at MBT-1, but were more prominently

affected by the transition to maximum interglacial warmth in both hemispheres at MBT-2 (Melles et

al., 2012; Li et al., 2017a). Meanwhile, the Asian winter monsoon did not change as prominently

across the MBT as the summer monsoon, as is indicated by limited responses in Chinese loess grain

size records across MIS 13 and MIS 11 (e.g., Ding et al., 2002; Sun et al., 2006; Hao et al., 2012).

Finally, stalagmite δ^{18}O records from South China warrant specific discussion. These records are

dominated by precession cycles with little evidence of 100-kyr glacial-interglacial cycles during the

past 640 kyr, and without major shifts at MIS 11 or MIS 13 (Cheng et al., 2016). These stalagmite

δ^{18}O variations have been interpreted as a record of East Asian summer monsoonal rainfall variability,

but are increasingly thought to be influenced not only by the monsoon, but also by other factors,

including moisture transportation distance, evaporation and condensation processes along the vapour

advection pathway, mixing of water vapour derived from different sources (Indian vs Pacific Ocean),

temperature changes at the moisture sources, glacial-interglacial seawater δ^{18}O variations, regional

temperature gradients, changes in seasonality and frontal position, and additional local effects (e.g.,

Maher and Thompson, 2012; Liu et al., 2015; Wang et al., 2017; Beck et al., 2018; Clemens et al.,

2018; Zhang et al., 2018). Full interpretation of different orbital features between Chinese loess and

South China stalagmite δ^{18}O records remains a challenge that has been debated extensively, and needs

further work. However, the apparent absence of MBT-1 and/or MBT-2 in some palaeoclimate records

(e.g., Ding et al., 2002; Tzedakis et al., 2006; Candy et al., 2010; An et al., 2011; Cheng et al., 2016) supports the concept that regionally differing climate imprints may be expected because of different regional response sensitivities to major climate rearrangements (Berger et al., 2016), and because individual records may record composite processes rather than a single process. This debate needs to be settled by further research using both observations and modelling.

4. Potential links between mid-Pleistocene environmental and human evolution

Integration of mid-Pleistocene palaeoclimatic and palaeoanthropological records provides an opportunity to obtain a global perspective on climate variability and human evolution across the MBT. Broadly, increased environmental extremes (cold/dry or warm/moist conditions) and resulting ecological and faunal changes have been suggested as likely drivers of hominin evolution over the past several million years (e.g., deMenocal, 1995, 2004; Potts, 1996; Potts et al., 2018). The shift to larger-amplitude glacial-interglacial variability across the two MBT stages between ~500 and 380 ka (MIS 13–11) corresponds to a critical time in human physical, behavioural, and genetic evolution, with the highest known diversification of human lineages/species occurring over this time interval (Galway-Witham et al., 2019) (Fig. 10). Starting from MBT-1 at ~500 ka, global archaeological records indicate prominent increases in new subsistence behaviour (e.g., fire control, large mammal butchery), technical innovations (e.g., improved core and Levallois technologies and increased light-duty tools), regionalization, and more intense social interactions (e.g., Roebroeks and Villa, 2011; Davis and Ashton, 2019; Galway-Witham et al., 2019; Biddittua et al., 2020; Moncel et al., 2020). We outline these major divergences below.

H. erectus, which is one of the first species of the *Homo* genus, expanded to low- and

mid-latitude Eurasia as early as ~1.8–1.6 Ma (Zhu et al., 2004, 2008, 2015; Dennell, 2009; Ferring et al., 2011; Ao et al., 2013b). It survived changing East Asian environments for more than one million years but seems to have disappeared in China after ~400 ka (Ao et al., 2017; Galway-Witham et al., 2019), close to MBT-2. Remaining *H. erectus* populations may then have been restricted to Southeast Asia, surviving in Java, where the tropical climate remained warm and wet. They persisted there despite increased climate variability across the MBT until ~100 ka (Galway-Witham et al., 2019; Rizal et al., 2019). It can be inferred that the ancestors of *H. floresiensis* were already present on the Indonesian island of Flores before MBT-1 because a related population is known there at ~700 ka (van den Bergh et al., 2016). Thus, it appears that *H. floresiensis* also survived increased Southeast Asian tropical climate variability across the MBT (van den Bergh et al., 2016) (Fig. 10). It can be inferred that the mid-Pleistocene species *H. heidelbergensis* was present at ~0.6 Ma in Europe and Africa from the German type fossil (Mauer) and key Ethiopian materials (Bodo) (Rightmire, 2009; Galway-Witham et al., 2019) (Fig. 10). It has often been considered as the likely last common ancestor of *H. neanderthalensis* and *H. sapiens* (Stringer, 2012a), but its evolutionary role is questionable now on both chronological and morphological grounds, and its extinction date is unknown (Gómez-Robles et al., 2013; Galway-Witham et al., 2019; Gómez-Robles, 2019; Grün et al., 2020).

The timespan across the two MBT stages encompasses the extinction of older lineages/species and the origination of new species and early divergences of old species in Europe, Asia, and Africa. This suggests a potential link between environmental change and human evolution (Fig. 10). Genetic calibrations using estimates of the autosomal human mutation rate suggest that the divergence date of the *H. neanderthalensis* and *H. sapiens* lineages could lie between ~550 and 765 ka or, alternatively,

18

between ~503 and 565 ka (Meyer et al., 2016; Hajdinjak et al., 2018). Given that genetic divergence precedes speciation, these lineages would have been differentiating during the MBT (Galway-Witham et al., 2019), between MIS 13 and 11. Another hominin group must have also begun its evolution by this time – the Denisovans, a sister group of Neanderthals. Denisovans are only known from Asian fossil evidence from the late mid-Pleistocene onward, but both genetic calibration and primitive morphological aspects compared with the Sima de los Huesos fossils from Atapuerca, Spain, place their divergence from the Neanderthal lineage earlier in the mid-Pleistocene, before ~430 ka (Reich et al., 2010; Jacobs et al., 2019). Although there is as yet no physical evidence, the origin of Denisovans from a common ancestor with Neanderthals probably occurred in East Asia during MIS 13–12. In the later mid-Pleistocene, China had a high morphological diversity of human populations, but apart from the Denisovan-related Xiahe mandible (~160 ka) in central China (Chen et al., 2019) and possible Denisovan fossils excavated from sites like Xujiayao (260–370 ka), North China (Ao et al., 2017), the affinities of "China archaics" like Chaoxian, Dali, and Jinniushan to other lineages, including the Denisovans, are also currently unclear (Ao et al., 2017; Galway-Witham et al., 2019). However, the suggested timing of the appearance of "China archaics" at ~400 ka (Ao et al., 2017) coincides with MBT-2. In addition, we can reasonably infer that the *H. naledi* lineage appeared in South Africa around or before the MBT (Galway-Witham et al., 2019). Although known fossil specimens are dated between 236 and 414 ka using a combination of optically stimulated luminescence (OSL) dating of sediments, U-Th and palaeomagnetic dating of flowstones, and U-series and electron spin resonance (US-ESR) dating of teeth (Dirks et al., 2017), the persistence of primitive traits suggests a much more ancient origin (Galway-Witham et al., 2019).

In both Europe and Africa, the period between ~500 and 400 ka is notable in terms of hominin

diversity, with brain sizes coming fully into the modern range for the first time. In Europe, this was a critical phase in the development of human evolution, technology, and societies (Davis and Ashton, 2019), and there was a range of fossil morphologies, with some attributed to early Neanderthals and others to the continuing *H. heidelbergensis* lineage (Stringer, 2012a; Manzi, 2016; Galway-Witham et al., 2019). For example, the extensive Sima de los Huesos sample can be placed on the Neanderthal lineage through numerous morphological traits, which is also supported by DNA analysis (Arsuaga et al., 2014; Meyer et al., 2016), while the penecontemporaneous braincase from Ceprano, Italy, has preponderantly primitive, rather than Neanderthal, traits (Manzi, 2016). Other fossils such as the calvaria from Gruta da Aureira, Portugal, have mixed features characteristic of European earlier middle Pleistocene crania (Daura et al., 2017). Experts differ in opinion on the most appropriate taxonomic and evolutionary allocation for these samples (e.g., Bermúdez De Castro et al., 2019; Rosas et al., 2019).

By ~600 ka, *H. heidelbergensis* was present in Africa as far apart as Ethiopia and South Africa, but subsequent climatic changes across the MBT could have produced niche contraction in a relatively drier southern Africa (Caley et al. 2018), while a more humid northern Africa (Rossignol-Strick et al., 1998; Geyh and Thiedig, 2008; Zhao et al., 2012) (Figs. 1 and 5) would have opened new niches for *H. heidelbergensis* population expansions with handaxe industries. In particular, northward expansion and intensification of the African monsoon (Rossignol-Strick et al., 1998; Zhao et al., 2012) may have transformed large parts of the Sahara Desert into a vegetated "green Sahara" savannah with large lakes (Geyh and Thiedig, 2008; Larrasoaña et al., 2013), which connected central Africa with the North African coast and with west Asia. It is not known whether *H. heidelbergensis* persisted in increasingly arid southern Africa (Fig. 5F), but it seemingly did so in Central and East Africa based on

evidence from Eyasi and Broken Hill (Dominguez-Rodrigo et al., 2008; Galway-Witham et al., 2019; Grün et al., 2020). It is possible that *H. naledi* differentiated in southern Africa as a more arid-adapted species with a lower quality diet following enhanced regional aridity across the MBT (Fig. 5F), but its evolutionary history and adaptations remain essentially unknown. *H. sapiens* may have emerged in Africa during the MBT at ~500–400 ka (Galway-Witham et al., 2019), which overlaps with the larger-amplitude MBT glacial-interglacial oscillations. The oldest recognized *H. sapiens* fossils are associated with Levallois artefacts (Middle Palaeolithic) from Jebel Irhoud, Morocco, dating between ~378 and 295 ka (Hublin et al., 2017; Richter et al., 2017) within the second full glacial to interglacial cycle of MIS 10–9. This date is younger than that of the MIS 12 early Neanderthals in Spain but is still within the larger-amplitude glacial-interglacial oscillations that followed MBT-2.

Along with increased amplitude of climate variability across the MBT, greater variation in lithic industries and hominin behaviour developed across Eurasia and Africa (Fig. 10). The two MBT stages coincided with behavioural changes leading toward the early Middle Palaeolithic, such as changes in cultures and land use patterns, and more versatile and standardized core technologies (Davis and Ashton, 2019; Biddittua et al., 2020). In Europe, handaxes were a major focus of stone tool manufacture before and during MIS 11 but became a more marginal technology or were absent after this time (Davis and Ashton, 2019). In East Asia, abundant handaxes appeared in central China from ~500 ka (Li et al., 2014), which might indicate that similar morphological and technological diversity was developing there. Levallois-like artefacts developed within MIS 12–9 in both Africa and Europe (Monnier, 2006; Hublin, 2009; Porat et al., 2010; Adler et al., 2014; Hublin et al., 2017; Richter et al., 2017; Potts et al., 2018; Moncel et al., 2020), which are markedly more technologically complex relative to the previous Lower Palaeolithic tools (including handaxes) and were probably more

efficient for hunting (Ambrose, 2010). The control and use of fire also becomes clearer in archaeological records from ~400 ka onward (Preece et al., 2006; Roebroeks and Villa, 2011; Ravon et al., 2016; Daura et al., 2017; Davis and Ashton, 2019), while the processing of hides for clothing and shelter may also have become widespread (Voormolen, 2008; Ashton, 2015). More persistent use of caves could also have facilitated the first regular construction of shelters (Olle et al., 2016; Ravon, 2018), leading to a growing recognition of place, space, and perhaps territories, which is critical for the structuring and operation of societies (Ashton, 2018; Ravon, 2018; Scott and Shaw, 2018). These lithic and behavioural developments may have potentially helped populations to adapt to the larger-amplitude climate variability.

It is apparent that many of these notable developments in human speciation, morphology, and behaviour coincided with the MBT. According to environmental theories of human evolution (e.g., deMenocal, 1995, 2004; Potts, 1996; Potts et al., 2018), this chronological match implies that the larger-amplitude climate variability across the MBT could have provided a driving force for the mid-Pleistocene high diversification of human lineages and behavioural changes. Generally, more extreme variability in precipitation (particularly in Africa) and temperature (particularly in Europe) had a global influence on human habitats, selection gradients, and biota, which may have impacted human survival, reproduction, and population sizes (Owen et al., 2018; Potts et al., 2018). Under favourable warm/humid conditions, resources were relatively abundant, and human populations probably increased in size, colonizing new regions (Dennell, 2009; Caley et al., 2018; Potts et al., 2018). Under less favourable cold/dry conditions, populations would have been prone to contraction, regional isolation or fragmentation, and even local extinction due to insufficient resource acquisition (e.g., food, water, and shelter), increased competition, and enhanced selective pressures (Dennell,

2009; Caley et al., 2018; Potts et al., 2018). Increased amplitudes of glacial-interglacial oscillations were also associated with prominent vegetation and mammalian community shifts across the MBT (e.g., Magri and Palombo, 2013; Head and Gibbard, 2015; Potts et al., 2018), which induced higher regional climate and ecosystem variability, and potentially increased foraging unpredictability (Hublin, 2009; Hublin and Roebroeks, 2009). Smaller numbers of human species, lower population density, and weaker social networks before MBT-1 at ~500 ka (Biddittua et al., 2020) would also have increased the likelihood of more isolated local populations becoming extinct under larger-amplitude climate variability and larger environmental stress after this time, particularly during the following "super" glacial MIS 12, when ice sheets first expanded south of 50°N in eastern and central Europe (Lauer and Weiss, 2018). For coeval human hunter-gatherers, the combined action of increased environmental and habitat variability, and unpredictable resource availability may have induced demographic crashes of some older human lineages (i.e., *H. erectus* and *H. heidelbergensis*) (Fig. 10). In addition to enhanced climatic adaptations, many surviving human populations could have been forced to widen their mobility, to increase planning depth and hunting proficiency, to share more information and resources, to extend regional social interaction and resource exchange networks with increased trust and cooperation, and to develop enhanced constructive memory, which would have enhanced adaptations to unpredicted selective pressures (Ambrose, 2010; Potts et al., 2018). These combinations may have improved fitness, increased encephalization, promoted novel hominin behaviour (e.g., fire control), pushed organized hunting to higher levels, enhanced foraging efficiency, and driven genetic drift or exchange (Hublin, 2009; Potts et al., 2018; Galway-Witham et al., 2019). Through these pressures and opportunities, some groups could have differentiated into distinct populations and then into new species. These possibilities and the evidence provided above of a

chronological correlation between environmental change and human evolution suggest that increased climate variability across the MBT may have provided a catalyst or appropriate conditions for evolution that induced the high diversification of human lineages (with coexisting distinct human groups) during the middle interval of the middle Pleistocene, including origination of Neanderthals, Denisovans, and *H. sapiens* (Fig. 10). This inference is consistent with environmental theories of human evolution (e.g., deMenocal, 1995, 2004; Potts, 1996; Potts et al., 2018) and provides a basis to elaborate on environmental and human co-evolution, although causal links between coeval climatic and evolutionary changes cross the MBT cannot yet be established.

The evolved new and surviving old species, coupled with technical and behavioural developments (e.g., Levallois tools and fire control) may have become more adaptable to increased environmental extremes (cold/dry or warm/moist conditions) across the MBT. In turn, this may have laid the foundation for subsequent episodic human expansions across Africa and Eurasia (Moncel et al., 2016; Davis and Ashton, 2019), including previously abandoned high-latitude Europe (subject to favourable conditions). More or less permanent occupation occurred in at least some of these regions, probably from "super" interglacial MIS 11 onward or even from the comparably regionally warm and wet European interglacial MIS 13 (Biddittua et al., 2020). Although occupation was punctuated by severe cold periods, particularly during the first "super" glacial MIS 12 between MBT-1 and MBT-2, which probably resulted in population decreases and niche contraction, there may have been near-continuous colonization in parts of southern Europe. The more maritime climates of northwestern Europe allowed occupation of northern latitudes for parts of this time, and it has been argued that this was a critical time for development of abilities to cope with long, cold winters (Ashton and Lewis, 2012; Cohen et al., 2012; Hosfield, 2016), although some earlier adaptations had

occurred – as indicated by human persistence in an Early Pleistocene boreal environment at Happisburgh 3 (Norfolk, UK; Parfitt et al., 2010). Shorter growing seasons would have demanded an obligate dependence on procuring meat, and several sites at this time provide greater evidence of the requisite technology (Roberts and Parfitt, 1999; Schoch et al., 2015).

5. Conclusions

Our palaeoclimatic synthesis suggests that the complete mid-brunhes climate transition was a two-stage process. The first stage (MBT-1) at ~500 ka was marked by increased temperature and precipitation over northern hemisphere continents during interglacial MIS 13, with accompanying global carbon cycle changes because of vegetation expansion. In the southern hemisphere, opposite temperature and precipitation changes are found during MBT-1. We relate the opposite precipitation changes between hemispheres to enhanced warming of northern hemisphere continents, limited southern hemisphere warming, and associated intensification and more extensive northward ITCZ swings. The second stage of the mid-brunhes climate transition (MBT-2) at ~400 ka was marked by a more global shift to greater interglacial warmth linked to increased atmospheric CO_2 concentrations, with reduced ice volume starting at MIS 11. The global shift to intensified interglacial conditions at MBT-2 was associated with sustained high interglacial precipitation in Asia from MIS 11 onward and with sustained high marine benthic $\delta^{13}C$ values during MIS 11.

Based on the observed temporal co-occurrence of environmental and human species changes, we infer that prominent climate changes across the MBT may have provided a catalyst or the appropriate conditions to promote mid-Pleistocene hominin and behavioural diversity. Relevant changes include human expansions across wider areas of Africa and Eurasia, longevity or extinction of older

lineages/species, origination of new species (e.g., emergence of Neanderthals in Europe, Denisovans in eastern and southeastern Eurasia, *H. sapiens* in Africa, and "China archaics" in East Asia), and the transition to Levallois technology in many regions. These observations are consistent with previous proposals of environmental influence on human evolution. Our hypothesis is testable with future development of a more complete understanding of mid-Pleistocene environmental changes, human lineage diversification, and behavioural developments. In particular, new palaeoanthropological data are needed from regions such as Africa and China, and from critical areas like the Indian subcontinent and much of southeastern Asia, which are marked by a near-complete lack of relevant materials.

Author contributions

H.A. conceived the study. H.A., P.Z., P.G.Y., and X.K.Q. performed multi-proxy measurements. H.A., E.J.R, Z.S.A., A.P.R., M.J.D., G.D.-N., O.S.L., Z.H.L., W.J.Z, W.H., G.Q.X., and Z.G.S. contributed to proxy analysis, interpretation, and discussion. C.S. contributed to palaeoanthropological interpretation. J.M.Y., X.L.M., and Z.D.J contributed to benthic δ^{13}C interpretation. X.Z.P and Q.S. helped on loess age model establishment. H.A., E.J.R, C.S., A.P.R., and Z.S.A. led the manuscript writing with intellectual contributions from all coauthors.

Acknowledgements

Data availability

All new data used in this study are attached in the Supplementary Dataset.

References

Adler, D.S., Wilkinson, K.N., Blockley, S., Mark, D.F., Pinhasi, R., Schmidt-Magee, B.A., Nahapetyan, S., Mallol, C., Berna, F., Glauberman, P.J., Raczynski-Henk, Y., Wales, N., Frahm, E., Joris, O., MacLeod, A., Smith, V.C., Cullen, V.L. and Gasparian, B., 2014. Early Levallois technology and the Lower to Middle Paleolithic transition in the Southern Caucasus. Science 345: 1609–1613.

Ambrose, S.H., 2010. Coevolution of composite-tool technology, constructive memory, and language. Curr. Anthropol. 51: 135–147.

An, Z.S., 2000. The history and variability of the East Asian paleomonsoon climate. Quat. Sci. Rev. 19: 171–187.

An, Z.S., 2014. Late Cenozoic Climate Change in Asia: Loess, Monsoon and Monsoon-Arid Environment Evolution. Springer, Amsterdam.

An, Z.S., Bowler, J.M., Opdyke, N.D., Macumber, P.G. and Firman, J.B., 1986. Paleomagnetic stratigraphy of Lake Bungunnia: Plio-Pleistocene precursor of aridity in the Murray Basin, southeastern Australia. Palaeogeogr. Palaeoclimatol. Palaeoecol. 54: 219–239.

An, Z.S. and Ho, C.K., 1989. New magnetostratigraphic dates of Lantian *Homo erectus*. Quat. Res. 32:

213–221.

An, Z.S., Liu, T.S., Lu, Y.C., Porter, S.C., Kukla, G., Wu, X.H. and Hua, Y.M., 1990. The long-term paleomonsoon variation recorded by the loess-paleosol sequence in central China. Quat. Int. 718: 91–95.

An, Z.S., Huang, Y.S., Liu, W.G., Guo, Z.T., Clemens, S., Li, L., Prell, W., Ning, Y.F., Cai, Y.J., Zhou, W.J., Lin, B.H., Zhang, Q.L., Cao, Y.N., Qiang, X.K., Chang, H. and Wu, Z.K., 2005. Multiple expansions of C_4 plant biomass in East Asia since 7 Ma coupled with strengthened monsoon circulation. Geology 33: 705–708.

An, Z.S., Clemens, S.C., Shen, J., Qiang, X.K., Jin, Z.D., Sun, Y.B., Prell, W.L., Luo, J.J., Wang, S.M., Xu, H., Cai, Y.J., Zhou, W.J., Liu, X.D., Liu, W.G., Shi, Z.G., Yan, L.B., Xiao, X.Y., Chang, H., Wu, F., Ai, L. and Lu, F.Y., 2011. Glacial-interglacial Indian summer monsoon dynamics. Science 333: 719–723.

Ao, H., Dekkers, M.J., Xiao, G.Q., Yang, X.Q., Qin, L., Liu, X.D., Qiang, X.K., Chang, H., and Zhao, H., 2012. Different orbital rhythms in the Asian summer monsoon records from North and South China during the Pleistocene. Global Planet. Change 80: 51–60.

Ao, H., An, Z.S., Dekkers, M.J., Li, Y.X., Xiao, G.Q., Zhao, H., Qiang, X.K., 2013a. Pleistocene magnetochronology of the fauna and Paleolithic sites in the Nihewan Basin: significance for environmental and hominin evolution in North China. Quat. Geochronol. 18: 78–92.

Ao, H., Dekkers, M.J., Wei, Q., Qiang, X.K., Xiao, G.Q., 2013b. New evidence for early presence of hominids in North China. Sci. Rep. 3: 2403, doi: 2410.1038/srep02403.

Ao, H., Liu, C.R., Roberts, A.P., Zhang, P. and Xu, X.W., 2017. An updated age for the Xujiayao hominin from the Nihewan Basin, North China: implications for Middle Pleistocene human

evolution in East Asia. J. Hum. Evol. 106: 54–65.

Arsuaga, J.L., Martínez, I., Arnold, L.J., Aranburu, A., Gracia-Téllez, A., Sharp, W.D., Quam, R.M., Falguères, C., Pantoja-Pérez, A., Bischoff, J., Poza-Rey, E., Parés, J.M., Carretero, J.M., Demuro, M., Lorenzo, C., Sala, N., Martinón-Torres, M., García, N., Alcázar de Velasco, A., Cuenca-Bescós, G., Gómez-Olivencia, A., Moreno, D., Pablos, A., Shen, C.C., Rodríguez, L., Ortega, A.I., García, R., Bonmatí, A., Bermúdez De Castro, J.M. and Carbonell, E., 2014. Neandertal roots: cranial and chronological evidence from Sima de los Huesos. Science 344: 1358–1363.

Ashton, N. and Lewis, S.G., 2012. The environmental contexts of early human occupation of northwest Europe: the British Lower Palaeolithic record. Quat. Int. 271: 50–64.

Ashton, N.M., 2015. Ecological niches, technological developments and physical adaptations of early humans in Europe: the handaxe-heidelbergensis hypothesis. In: Wenban-Smith, F., Coward, F. and Hosfield, R. (Editors), Settlement, Society and Cognition in Human Evolution: Landscapes in Mind. Cambridge Univ. Press, New York, pp. 138–153.

Ashton, N.M., 2018. Landscapes of habit and persistent places during MIS 11 in Europe: a return journey from Britain. In: Pope, M., McNabb, J. and Gamble, C.B. (Editors), Crossing the Human Threshold: Dynamic Transformation and Persistent Places during the Middle Pleistocene. Routledge, London, pp. 142–164.

Augustin, L., Barbante, C., Barnes, P.R.F., Barnola, J.M., Bigler, M., Castellano, E., Cattani, O., Chappellaz, J., DahlJensen, D., Delmonte, B., Dreyfus, G., Durand, G., Falourd, S., Fischer, H., Flückiger, J., Hansson, M.E., Huybrechts, P., Jugie, R., Johnsen, S.J., Jouzel, J., Kaufmann, P., Kipfstuhl, J., Lambert, F., Lipenkov, V.Y., Littot, G.V.C., Longinelli, A., Lorrain, R., Maggi, V.,

Masson-Delmotte, V., Miller, H., Mulvaney, R., Oerlemans, J., Oerter, H., Orombelli, G., Parrenin, F., Peel, D.A., Petit, J.R., Raynaud, D., Ritz, C., Ruth, U., Schwander, J., Siegenthaler, U., Souchez, R., Stauffer, B., Steffensen, J.P., Stenni, B., Stocker, T.F., Tabacco, I.E., Udisti, R., van de Wal, R.S.W., van den Broeke, M., Weiss, J., Wilhelms, F., Winther, J.G., Wolff, E.W. and Zucchelli, M., 2004. Eight glacial cycles from an Antarctic ice core. Nature 429: 623–628.

Beck, J.W., Zhou, W.J., Li, C., Wu, Z.K., White, L., Xian, F., Kong, X.H., An, Z.S., 2018. A 550,000-year record of East Asian monsoon rainfall from ^{10}Be in loess. Science 360, 877–881.

Berger, A., Crucifix, M., Hodell, D.A., Mangili, C., McManus, J.F., Otto-Bliesner, B., Pol, K., Raynaud, D., Skinner, L.C., Tzedakis, P.C., Wolff, E.W., Yin, Q.Z., Abe-Ouchi, A., Barbante, C., Brovkin, V., Cacho, I., Capron, E., Ferretti, P., Ganopolski, A., Grimalt, J.O., Hönisch, B., Kawamura, K., Landais, A., Margari, V., Martrat, B., Masson-Delmotte, V., Mokeddem, Z., Parrenin, F., Prokopenko, A.A., Rashid, H., Schulz, M., and Riveiros, N.V., 2016. Interglacials of the last 800,000 years. Rev. Geophys. 54: 162–219.

Bermúdez De Castro, J.M., Martinon-Torres, M., de Pinillos, M.M., García-Campos, C., Modesto-Mata, M., Martín-Frances, L. and Arsuaga, J.L., 2019. Metric and morphological comparison between the Arago (France) and Atapuerca-Sima de los Huesos (Spain) dental samples, and the origin of Neanderthals. Quat. Sci. Rev. 217: 45–61.

Biddittua, I., Moncelb, M.H., Millic, S., Belluccia, L., Ruffoa, M., Saracinoa, B. and Manzi, G., 2020. Stratigraphy, sedimentology, and archaeology of Middle Pleistocene localities near Ceprano, Campogrande area, Italy. Quat. Res. 93: doi: 10.1017/qua.2019.52.

Blain, H.A., Cuenca-Bescós, G., Lozano-Fernández, I., López-García, J.M., Ollé, A., Rosell, J. and

Rodríguez, J., 2012. Investigating the Mid-Brunhes Event in the Spanish terrestrial sequence. Geology 40: 1051–1054.

Caley, T., Kim, J.H., Malaize, B., Giraudeau, J., Laepple, T., Caillon, N., Charlier, K., Rebaubier, H., Rossignol, L., Castaneda, I.S., Schouten, S. and Damste, J.S.S., 2011. High-latitude obliquity as a dominant forcing in the Agulhas current system. Clim. Past 7: 1285–1296.

Caley, T., Extier, T., Collins, J.A., Schefuss, E., Dupont, L., Malaize, B., Rossignol, L., Souron, A., McClymont, E.L., Jimenez-Espejo, F.J., Garcia-Comas, C., Eynaud, F., Martinez, P., Roche, D.M., Jorry, S.J., Charlier, K., Wary, M., Gourves, P.Y., Billy, I. and Giraudeau, J., 2018. A two-million-year-long hydroclimatic context for hominin evolution in southeastern Africa. Nature 560: 76–79.

Candy, I., Coope, G.R., Lee, J.R., Parfitt, S.A., Preece, R.C., Rose, J. and Schreve, D.C., 2010. Pronounced warmth during early Middle Pleistocene interglacials: investigating the Mid-Brunhes Event in the British terrestrial sequence. Earth-Sci. Rev. 103: 183–196

Candy, I. and McClymont, E.L., 2013. Interglacial intensity in the North Atlantic over the last 800 000 years: investigating the complexity of the mid-Brunhes Event. J. Quat. Sci. 28: 343–348.

Chen, F.H., Bloemendal, J., Zhang, P.Z. and Liu, G.X., 1999. An 800 ky proxy record of climate from lake sediments of the Zoige Basin, eastern Tibetan Plateau. Palaeogeogr. Palaeoclimatol. Palaeoecol. 151: 307–320.

Chen, F.H., Welker, F., Shen, C.C., Bailey, S.E., Bergmann, I., Davis, S., Xia, H., Wang, H., Fischer, R., Freidline, S.E., Yu, T.L., Skinner, M.M., Stelzer, S., Dong, G.R., Fu, Q.M., Dong, G.H., Wang, J., Zhang, D.J. and Hublin, J.J., 2019. A late Middle Pleistocene Denisovan mandible from the Tibetan Plateau. Nature 569: 409–412.

Cheng, H., Edwards, R.L., Sinha, A., Spotl, C., Yi, L., Chen, S.T., Kelly, M., Kathayat, G., Wang, X.F., Li, X.L., Kong, X.G., Wang, Y.J., Ning, Y.F. and Zhang, H.W., 2016. The Asian monsoon over the past 640,000 years and ice age terminations. Nature 534: 640–646.

Chiang, J.C.H. and Bitz, C.M., 2005. Influence of high latitude ice cover on the marine Intertropical Convergence Zone. Clim. Dyn. 25: 477–496.

Clemens, S.C., Murray, D.W. and Prell, W.L., 1996. Nonstationary phase of the Plio-Pleistocene Asian monsoon. Science 274: 943–948.

Clemens, S.C., Holbourn, A., Kubota, Y., Lee, K.E., Liu, Z., Chen, G., Nelson, A. and Fox-Kemper, B., 2018. Precession-band variance missing from East Asian monsoon runoff. Nature Commun. 9: 3364, doi: 10.1038/s41467-018-05814-0.

Cohen, K.M., MacDonald, K., Joordens, J.C.A., Roebroeks, W. and Gibbard, P.L., 2012. The earliest occupation of north-west Europe: a coastal perspective. Quat. Int. 271: 70–83.

Combourieu-Nebout, N., Bertini, A., Russo-Ermolli, E., Peyron, O., Klotz, S., Montade, V., Fauquette, S., Allen, J., Fusco, F., Goring, S., Huntley, B., Joannin, S., Lebreton, V., Magri, D., Martinetto, E., Orain, R. and Sadori, L. 2015. Climate changes in the central Mediterranean and Italian vegetation dynamics since the Pliocene. Rev. Palaeobot. Palynol. 218: 127–147.

Contreras, S., Werne, J.P., Brown, E.T., Anderson, R.S. and Fawcett, P.J., 2016. A molecular isotope record of climate variability and vegetation response in southwestern North America during mid-Pleistocene glacial/interglacial cycles. Palaeogeogr. Palaeoclimatol. Palaeoecol. 459: 338–347.

Daura, J., Sanz, M., Arsuaga, J.L., Hoffmann, D.L., Quam, R.M., Ortega, M.C., Santos, E., Gomez, S., Rubio, A., Villaescusa, L., Souto, P., Mauricio, J., Rodrigues, F., Ferreira, A., Godinho, P.,

Trinkaus, E. and Zilhao, J., 2017. New Middle Pleistocene hominin cranium from Gruta da Aroeira (Portugal). Proc. Natl. Acad. Sci. U. S. A. 114: 3397–3402.

Davis, R. and Ashton, N., 2019. Landscapes, environments and societies: the development of culture in Lower Palaeolithic Europe. J. Anthropol. Archaeol. 56: 101107, doi: 10.1016/j.jaa.2019.101107.

de Vernal, A. and Hillaire-Marcel, C., 2008. Natural variability of Greenland climate, vegetation, and ice volume during the past million years. Science 320: 1622–1625.

deMenocal, P.B., 1995. Plio-Pleistocene African climate. Science 270: 53–59.

deMenocal, P.B., 2004. African climate change and faunal evolution during the Pliocene–Pleistocene. Earth Planet. Sci. Lett. 220: 3–24.

Dennell, R.W., 2009. The Palaeolithic Settlement of Asia. Cambridge Univ. Press, New York, 572 pp.

Ding, Z.L., Derbyshire, E., Yang, S.L., Yu, Z.W., Xiong, S.F. and Liu, T.S., 2002. Stacked 2.6-Ma grain size record from the Chinese loess based on five sections and correlation with the deep-sea $\delta^{18}O$ record. Paleoceanography 17: 1033, doi: 10.1029/2001PA000725.

Dirks, P.H.G.M., Roberts, E.M., Hilbert-Wolf, H., Kramers, J.D., Hawks, J., Dosseto, A., Duval, M., Elliott, M., Evans, M., Grün, R., Hellstrom, J., Herries, A.I.R., Joannes-Boyau, R., Makhubela, T.V., Placzek, C.J., Robbins, J., Spandler, C., Wiersma, J., Woodhead, J. and Berger, L.R., 2017. The age of *Homo naledi* and associated sediments in the Rising Star Cave, South Africa. Elife 6: e24231, doi: 10.7554/eLife.24231.

Dominguez-Rodrigo, M., Mabulla, A., Luque, L., Thompson, J.W., Rink, J., Bushozi, P., Diez-Martin, F. and Alcala, L., 2008. A new archaic *Homo sapiens* fossil from Lake Eyasi, Tanzania. J. Hum. Evol. 54: 899–903.

33

Elderfield, H., Ferretti, P., Greaves, M., Crowhurst, S., McCave, I.N., Hodell, D. and Piotrowski, A.M., 2012. Evolution of ocean temperature and ice volume through the Mid-Pleistocene climate transition. Science 337: 704–709.

Etourneau, J., Martinez, P., Blanz, T. and Schneider, R., 2009. Pliocene–Pleistocene variability of upwelling activity, productivity, and nutrient cycling in the Benguela region. Geology 37: 871–874.

Farmer, J.R., Hönisch, B., Haynes, L.L., Kroon, D., Jung, S., Ford, H.L., Raymo, M.E., Jaume-Seguí, M., Bell, D.B., Goldstein, S.L., Pena, L.D., Yehudai, M. and Kim, J., 2019. Deep Atlantic Ocean carbon storage and the rise of 100,000-year glacial cycles. Nat. Geosci. 12: 355–360.

Fawcett, P.J., Werne, J.P., Anderson, R.S., Heikoop, J.M., Brown, E.T., Berke, M.A., Smith, S.J., Goff, F., Donohoo-Hurley, L., Cisneros-Dozal, L.M., Schouten, S., Damste, J.S.S., Huang, Y.S., Toney, J., Fessenden, J., WoldeGabriel, G., Atudorei, V., Geissman, J.W. and Allen, C.D., 2011. Extended megadroughts in the southwestern United States during Pleistocene interglacials. Nature 470: 518–521.

Ferring, R., Oms, O., Agustí, J., Berna, F., Nioradze, M., Shelia, T., Tappen, M., Vekua, A., Zhvania, D., Lordkipanidze, D., 2011. Earliest human occupations at Dmanisi (Georgian Caucasus) dated to 1.85–1.78 Ma. Proc. Natl. Acad. Sci. U. S. A., 10432–10436.

Galway-Witham, J., Cole, J. and Stringer, C., 2019. Aspects of human physical and behavioural evolution during the last 1 million years. J. Quat. Sci. 34: 355–378.

Geyh, M.A. and Thiedig, F., 2008. The Middle Pleistocene Al Mahrúqah Formation in the Murzuq Basin, northern Sahara, Libya evidence for orbitally-forced humid episodes during the last 500,000 years. Palaeogeogr. Palaeoclimatol. Palaeoecol. 257: 1–21.

Gingele, F.X. and Schmieder, F., 2001. Anomalous South Atlantic lithologies confirm global scale of unusual mid-Pleistocene climate excursion. Earth Planet. Sci. Lett. 186: 93–101.

Gómez-Robles, A., 2019. Dental evolutionary rates and its implications for the Neanderthal-modern human divergence. Sci. Adv. 5: eaaw1268.

Gómez-Robles, A., Bermúdez de Castro, J.M., Arsuaga, J.L., Carbonell, E. and Polly, P.D., 2013. No known hominin species matches the expected dental morphology of the last common ancestor of Neanderthals and modern humans. Proc. Natl. Acad. Sci. U. S. A. 110: 18196–18201.

Grant, K.M., Rohling, E.J., Ramsey, C.B., Cheng, H., Edwards, R.L., Florindo, F., Heslop, D., Marra, F., Roberts, A.P., Tamisiea, M.E., Williams, F., 2014. Sea-level variability over five glacial cycles. Nat. Commun. 5, 5076: doi: 5010.1038/ncomms6076.

Grün, R., Pike, A., McDermott, F., Eggins, S., Mortimer, G., Aubert, M., Kinsley, L., Joannes-Boyau, R., Rumsey, M., Denys, C., Brink, J., Clark, T., Stringer, C., 2020. Dating the skull from Broken Hill, Zambia, and its position in human evolution. Nature 580: doi: 10.1038/s41586-41020-42165-41584.

Guo, Z.T., Ruddiman, W.F., Hao, Q.Z., Wu, H.B., Qiao, Y.S., Zhu, R.X., Peng, S.Z., Wei, J.J., Yuan, B.Y., Liu, T.S., 2002. Onset of Asian desertification by 22 Myr ago inferred from loess deposits in China. Nature 416: 159–163.

Guo, Z.T., Berger, A., Yin, Q.Z. and Qin, L., 2009. Strong asymmetry of hemispheric climates during MIS-13 inferred from correlating China loess and Antarctica ice records. Clim. Past 5: 21–31.

Hajdinjak, M., Fu, Q.M., Hübner, A., Petr, M., Mafessoni, F., Grote, S., Skoglund, P., Narasimham, V., Rougier, H., Crevecoeur, I., Semal, P., Soressi, M., Talamo, S., Hublin, J.J., Gušić, I., Kucan, Z., Rudan, P., Golovanova, L.V., Doronichev, V.B., Posth, C., Krause, J., Korlević, P., Nagel,

S., Nickel, B., Slatkin, M., Patterson, N., Reich, D., Prüfer, K., Meyer, M., Pääbo, S. and Kelso, J., 2018. Reconstructing the genetic history of late Neanderthals. Nature 555: 652–656.

Hao, Q.Z., Wang, L., Oldfield, F., Peng, S.Z., Qin, L., Song, Y., Xu, B., Qiao, Y.S., Bloemendal, J. and Guo, Z.T., 2012. Delayed build-up of Arctic ice sheets during 400,000-year minima in insolation variability. Nature 490: 393–396.

Harris, S.E., Mix, A. and King, T., 1997. Biogenic and terrigenous sedimentation at Ceara Rise, western tropical Atlantic, supports Pliocene-Pleistocene deep-water linkage between hemsipheres. Proc. ODP Sci. Res. 154: 331–345.

Head, M.J. and Gibbard, P.L., 2015. Early–Middle Pleistocene transitions: linking terrestrial and marine realms. Quat. Int. 389: 7–46.

Herries, A.I.R., Martin, J.M., Leece, A.B., Adams, J.W., Boschian, G., Joannes-Boyau, R., Edwards, T.R., Mallett, T., Massey, J., Murszewski, A., Neubauer, S., Pickering, R., Strait, D.S., Armstrong, B.J., Baker, S., Caruana, M.V., Denham, T., Hellstrom, J., Moggi-Cecchi, J., Mokobane, S., Penzo-Kajevski, P., Rovinsky, D.S., Schwartz, G.T., Stammers, R.C., Wilson, C., Woodhead, J. and Menter, C., 2020. Contemporaneity of *Australopithecus*, *Paranthropus*, and early *Homo erectus* in South Africa. Science, 368: doi: 10.1126/science.aaw7293.

Heslop, D., Langereis, C.G. and Dekkers, M.J., 2000. A new astronomical timescale for the loess deposits of Northern China. Earth Planet. Sci. Lett. 184: 125–139.

Hodell, D.A., Kanfoush, S.L., Venz, K.A., Charles, C.D. and Sierro, F.J., 2013. The mid-Brunhes transition in ODP sites 1089 and 1090 (subantarctic South Atlantic). AGU Geophys. Monogr. 137: 113–129.

Holden, P.B., Edwards, N.R., Wolff, E.W., Valdes, P.J. and Singarayer, J.S., 2011. The mid-Brunhes

event and West Antarctic ice sheet stability. J. Quat. Sci. 26: 474–477.

Hoogakker, B.A.A., Rohling, E.J., Palmer, M.R., Tyrrell, T. and Rothwell, R.G., 2006. Underlying causes for long-term global ocean δ^{13}C fluctuations over the last 1.20 Myr. Earth Planet. Sci. Lett. 248: 15–29.

Hooghiemstra, H. and Ran, E.T.H., 1994. Late and Middle Pleistocene climatic-change and forest development in Colombia–pollen record Funza-Ii (2–158m core interval). Palaeogeogr. Palaeoclimatol. Palaeoecol. 109: 211–246.

Horikawa, K., Murayama, M., Minagawa, M., Kato, Y. and Sagawa, T., 2010. Latitudinal and downcore (0–750 ka) changes in n-alkane chain lengths in the eastern equatorial Pacific. Quat. Res. 73: 573–582.

Hosfield, R., 2016. Walking in a winter wonderland? Strategies for Early and Middle Pleistocene survival in midlatitude Europe. Curr. Anthropol. 57: 653–682.

Howe, J.N.W. and Piotrowski, A.M., 2017. Atlantic deep water provenance decoupled from atmospheric CO_2 concentration during the lukewarm interglacials. Nat. Commun. 8: 2003, doi: 10.1038/s41467/017/01939/w.

Hublin, J.J., 2009. The origin of Neandertals. Proc. Natl. Acad. Sci. U. S. A. 106: 16022–16027.

Hublin, J.J. and Roebroeks, W., 2009. Ebb and flow or regional extinctions? On the character of Neandertal occupation of northern environments. C. R. Palevol. 8: 503–509.

Hublin, J.J., Ben-Ncer, A., Bailey, S.E., Freidline, S.E., Neubauer, S., Skinner, M.M., Bergmann, I., Le Cabec, A., Benazzi, S., Harvati, K. and Gunz, P., 2017. New fossils from Jebel Irhoud, Morocco and the pan-African origin of *Homo sapiens*. Nature 546: 289–292.

Ivory, S.J., Blome, M.W., King, J.W., McGlue, M.M., Cole, J.E. and Cohen, A.S., 2016.

Environmental change explains cichlid adaptive radiation at Lake Malawi over the past 1.2 million years. Proc. Natl. Acad. Sci. U. S. A. 113: 11895–11900.

Jaccard, S.L., Hayes, C.T., Martinez-Garcia, A., Hodell, D.A., Anderson, R.F., Sigman, D.M. and Haug, G.H., 2013. Two modes of change in Southern Ocean productivity over the past million years. Science 339: 1419–1423.

Jacobs, G.S., Hudjashov, G., Saag, L., Kusuma, P., Darusallam, C.C., Lawson, D.J., Mondal, M., Pagani, L., Ricaut, F.X., Stoneking, M., Metspalu, M., Sudoyo, H., Lansing, J.S. and Cox, M.P., 2019. Multiple deeply divergent Denisovan ancestries in Papuans. Cell 177: 1010–1021.

Jansen, J.H.F., Kuijpers, A. and Troelstra, S.R., 1986. A mid-Brunhes climatic event: long-term changes in global atmosphere and ocean circulation. Science 232: 619–622.

Jouzel, J., Masson-Delmotte, V., Cattani, O., Dreyfus, G., Falourd, S., Hoffmann, G., Minster, B., Nouet, J., Barnola, J.M., Chappellaz, J., Fischer, H., Gallet, J.C., Johnsen, S., Leuenberger, M., Loulergue, L., Luethi, D., Oerter, H., Parrenin, F., Raisbeck, G., Raynaud, D., Schilt, A., Schwander, J., Selmo, E., Souchez, R., Spahni, R., Stauffer, B., Steffensen, J.P., Stenni, B., Stocker, T.F., Tison, J.L., Werner, M. and Wolff, E.W., 2007. Orbital and millennial Antarctic climate variability over the past 800,000 years. Science 317: 793–796.

Kunkelova, T., Jung, S.J.A., de Leau, E.S., Odling, N., Thomas, A.L., Betzler, C., Eberli, G.P., Alvarez-Zarikian, C.A., Alonso-Garcia, M., Bialik, O.M., Blattler, C.L., Guo, J.A., Haffen, S., Horozal, S., Mee, A.L.H., Inoue, M., Jovane, L., Lanci, L., Laya, J.C., Ludmann, T., Bejugam, N.N., Nakakuni, M., Niino, K., Petruny, L.M., Pratiwi, S.D., Reijmer, J.J.G., Reolid, J., Slagle, A.L., Sloss, C.R., Su, X., Swart, P.K., Wright, J.D., Yao, Z.Q., Young, J.R., Lindhorst, S., Stainbank, S., Rueggeberg, A., Spezzaferri, S., Carrasqueira, I., Hu, S. and Kroon, D., 2018. A

two million year record of low-latitude aridity linked to continental weathering from the Maldives. Prog. Earth Planet. Sci. 5: doi: 10.1186/s40645-018-0238-x

Lang, N. and Wolff, E.W., 2011. Interglacial and glacial variability from the last 800 ka in marine, ice and terrestrial archives. Clim. Past 7: 361–380.

Larrasoaña, J.C., Roberts, A.P. and Rohling, E.J., 2013. Dynamics of green Sahara periods and their role in Hominin evolution. Plos One 8: doi: 10.1371/journal.pone.0076514

Lauer, T. and Weiss, M., 2018. Timing of the Saalian- and Elsterian glacial cycles and the implications for Middle-Pleistocene hominin presence in central Europe. Sci. Rep. 8: 5111: doi: 10.1038/s41598-018-23541-w.

Lear, C.H., Billups, K., Rickaby, R.E.M., Diester-Haass, L., Mawbey, E.M. and Sosdian, S.M., 2016. Breathing more deeply: deep ocean carbon storage during the mid-Pleistocene climate transition. Geology 44: 1035–1038.

Li, H., Li, C.R., Kuman, K., Cheng, J., Yao, H.T. and Li, Z., 2014. The Middle Pleistocene handaxe site of Shuangshu in the Danjiangkou Reservoir Region, central China. J. Archaeol. Sci. 52: 391–409.

Li, L., Li, Q.Y., Tian, J., Wang, H. and Wang, P.X., 2013. Low latitude hydro-climatic changes during the Plio-Pleistocene: evidence from high resolution alkane records in the southern South China Sea. Quat. Sci. Rev. 78: 209–224.

Li, X.L., Hao, Q.Z., Wei, M.J., Andreev, A.A., Wang, J.P., Tian, Y.Y., Li, X.L., Cai, M.T., Hu, J.M. and Shi, W., 2017a. Phased uplift of the northeastern Tibetan Plateau inferred from a pollen record from Yinchuan Basin, northwestern China. Sci. Rep. 7: 18023, doi: 10.1038/s41598-017-16915-z.

Li, X.W., Ao, H., Dekkers, M.J., Roberts, A.P., Zhang, P., Lin, S., Huang, W.W., Hou, Y.M., Zhang, W.H. and An, Z.S., 2017b. Early Pleistocene occurrence of Acheulian technology in North China. Quat. Sci. Rev. 156: 12–22.

Lisiecki, L.E. and Raymo, M.E., 2005. A Pliocene-Pleistocene stack of 57 globally distributed benthic $\delta^{18}O$ records. Paleoceanography 20: PA1003, doi: 10.1029/2004PA001071.

Litt, T., Pickarski, N., Heumann, G., Stockhecke, M. and Tzedakis, P.C., 2014. A 600,000 year long continental pollen record from Lake Van, eastern Anatolia (Turkey). Quat. Sci. Rev. 104: 30–41.

Liu, J.B., Chen, J.H., Zhang, X.J., Li, Y., Rao, Z.G. and Chen, F.H., 2015. Holocene East Asian summer monsoon records in northern China and then inconsistency with Chinese stalagmite $\delta^{18}O$ records. Earth-Sci. Rev. 148: 194–208.

Lu, H., Yin, Q.Z., Jia, J., Xia, D.S., Gao, F.Y., Lyu, A., Ma, Y.P. and Yang, F., 2020. Possible link of an exceptionally strong East Asian summer monsoon to a La Niña-like condition during the interglacial MIS-13. Quat. Sci. Rev. 227, doi: 10.1016/j.quascirev.2019.106048.

Lüthi, D., Le Floch, M., Bereiter, B., Blunier, T., Barnola, J.M., Siegenthaler, U., Raynaud, D., Jouzel, J., Fischer, H., Kawamura, K. and Stocker, T.F., 2008. High-resolution carbon dioxide concentration record 650,000–800,000 years before present. Nature 453: 379–382.

Maher, B.A., 1998. Magnetic properties of modern soils and Quaternary loessic paleosols: paleoclimatic implications. Palaeogeogr. Palaeoclimatol. Palaeoecol. 137: 25–54.

Maher, B.A., 2016. Palaeoclimatic records of the loess/palaeosol sequences of the Chinese Loess Plateau. Quat. Sci. Rev. 154: 23–84.

Maher, B.A. and Thompson, R., 1995. Paleorainfall reconstructions from pedogenic magnetic

susceptibility variations in the Chinese loess and paleosols. Quat. Res. 44: 383–391.

Maher, B.A. and Thompson, R., 2012. Oxygen isotopes from Chinese caves: records not of monsoon rainfall but of circulation regime. J. Quat. Sci. 27: 615–624.

Magri, D. and Palombo, M.R., 2013. Early to Middle Pleistocene dynamics of plant and mammal communities in South West Europe. Quat. Int. 288: 63–72.

Manzi, G., 2016. Humans of the Middle Pleistocene: the controversial calvarium from Ceprano (Italy) and its significance for the origin and variability of *Homo heidelbergensis*. Quat. Int. 411: 254–261.

Margari, V., Roucoux, K., Magri, D., Manzi, G. and Tzedakis, P.C., 2018. The MIS 13 interglacial at Ceprano, Italy, in the context of Middle Pleistocene vegetation changes in southern Europe. Quat. Sci. Rev. 199: 144–158.

Marković, S.B., Stevens, T., Kukla, G.J., Hambach, U., Fitzsimmons, K.E., Gibbard, P., Buggle, B., Zech, M., Guo, Z.T., Hao, Q.Z., Wu, H.B., Dhand, K.O., Smalley, I.J., Újvári, G., Sümegi, P., Timar-Gabor, A., Veres, D., Sirocko, F., Vasiljević, D.A., Jary, Z., Svensson, A., Jović, V., Lehmkuhl, F., Kovács, J. and Svirčev, Z., 2015. Danube loess stratigraphy – towards a pan-European loess stratigraphic model. Earth-Sci. Rev. 148: 228–258.

Martínez-Botí, M.A., Foster, G.L., Chalk, T.B., Rohling, E.J., Sexton, P.F., Lunt, D.J., Pancost, R.D., Badger, M.P.S. and Schmidt, D.N., 2015. Plio-Pleistocene climate sensitivity evaluated using high-resolution CO_2 records. Nature 518: 49–54.

Martínez-Garcia, A., Rosell-Melé, A., Geibert, W., Gersonde, R., Masqué, P., Gaspari, V. and Barbante, C., 2009. Links between iron supply, marine productivity, sea surface temperature, and CO_2 over the last 1.1 Ma. Paleoceanography 24: PA1207, doi: 10.1029/2008PA001657.

Medina-Elizalde, M. and Lea, D.W., 2005. The mid-Pleistocene transition in the tropical Pacific. Science 310: 1009–1012.

Melles, M., Brigham-Grette, J., Minyuk, P.S., Nowaczyk, N.R., Wennrich, V., DeConto, R.M., Anderson, P.M., Andreev, A.A., Coletti, A., Cook, T.L., Haltia-Hovi, E., Kukkonen, M., Lozhkin, A.V., Rosen, P., Tarasov, P., Vogel, H. and Wagner, B., 2012. 2.8 million years of Arctic climate change from Lake El'gygytgyn, NE Russia. Science 337: 315–320.

Meyer, M., Arsuaga, J.L., de Filippo, C., Nagel, S., Aximu-Petri, A., Nickel, B., Martínez, I., Gracia, A., Bermúdez de Castro, J.M., Carbonell, E., Viola, B., Kelso, J., Prüfer, K. and Pääbo, S., 2016. Nuclear DNA sequences from the Middle Pleistocene Sima de los Huesos hominins. Nature 531: 504–507.

Mix, A.C., Pisias, N.G., Rugh, W., Wilson, J., Morey, A. and Hagelberg, T.K., 1995. Benthic foraminifer stable isotope record from Site 849 (0–5 Ma): local and global climate changes. Proc. ODP Sci. Res. 138: 371–412

Moncel, M.H., Arzarello, M. and Peretto, C., 2016. The Hoslteinian period in Europe (MIS 11–9). Quat. Int. 409: 1–8.

Moncel, M.H., Ashton, N., Arzarello, M., Fontana, F., Lamotte, A., Scott, B., Muttillo, B., Berruti, G., Nenzioni, G., Tuffreau, A. and Peretto, C., 2020. Early Levallois core technology between Marine Isotope Stage 12 and 9 in Western Europe. J. Hum. Evol. 139: doi: 10.1016/j.jhevol.2019.102735

Monnier, G.F., 2006. The Lower/Middle Paleolithic periodization in western Europe: an evaluation. Curr. Anthropol. 47: 709–744.

Murray, R.W., Leinen, M. and Knowlton, C.W., 2012. Links between iron input and opal deposition in

the Pleistocene equatorial Pacific Ocean. Nat. Geosci. 5: 270–274.

Olle, A., Mosquera, M., Rodriguez-Alvarez, X.P., Garcia-Medrano, P., Barsky, D., de Lombera-Hermida, A. and Carbonell, E., 2016. The Acheulean from Atapuerca: three steps forward, one step back. Quat. Int. 411: 316–328.

Owen, R.B., Muiruri, V.M., Lowenstein, T.K., Renaut, R.W., Rabideaux, N., Luo, S.D., Deino, A.L., Sier, M.J., Dupont-Nivet, G., McNulty, E.P., Leet, K., Cohen, A., Campisano, C., Deocampo, D., Shen, C.C., Billingsley, A. and Mbuthia, A., 2018. Progressive aridification in East Africa over the last half million years and implications for human evolution. Proc. Natl. Acad. Sci. U. S. A. 115: 11174–11179.

Parfitt, S.A., Ashton, N.M., Lewis, S.G., Abel, R.L., Coope, G.R., Field, M.H., Gale, R., Hoare, P.G., Larkin, N.R., Lewis, M.D., Karloukovski, V., Maher, B.A., Peglar, S.M., Preece, R.C., Whittaker, J.E. and Stringer, C.B., 2010. Early Pleistocene human occupation at the edge of the boreal zone in northwest Europe. Nature 466: 229–233.

Pollard, D. and Deconto, R.M., 2009. Modelling West Antarctic ice sheet growth and collapse through the past five million years. Nature 458: 329–332.

Polyak, L., Best, K.M., Crawford, K.A., Council, E.A. and StOnge, G., 2013. Quaternary history of sea ice in the western Arctic Ocean based on foraminifera. Quat. Sci. Rev. 79: 145–156.

Porat, M., Chazan, R., Grün, R., Aubert, M., Eisenmann, V. and Horwitz, L.K., 2010. New radiometric ages for the Fauresmith industry from Kathu Pan, southern Africa: implications for the Earlier to Middle Stone Age transition. J. Archaeol. Sci. 37: 269–283.

Porter, S.C. and An, Z.S., 1995. Correlation between climate events in the North Atlantic and China during the last glaciation. Nature 375: 305–308.

Potts, R., 1996. Evolution and climate variability. Science 273: 922–923.

Potts, R., Behrensmeyer, A.K., Faith, J.T., Tryon, C.A., Brooks, A.S., Yellen, J.E., Deino, M.L., Kinyanjui, R., Clark, J.B., Haradon, C.M., Levin, N.E., Meijer, H.J.M., Veatch, E.G., Owen, R.B. and Renaut, R.W., 2018. Environmental dynamics during the onset of the Middle Stone Age in eastern Africa. Science 360: 86–90.

Preece, R.C., Gowlett, J.A.J., Parfitt, S.A., Bridgland, D.R. and Lewis, S.G., 2006. Humans in the Hoxnian: habitat, context and fire use at Beeches Pit, West Stow, Suffolk, UK. J. Quat. Sci. 21: 485–496.

Prokopenko, A.A., Williams, D.F., Kuzmin, M.I., Karabanov, E.B., Khursevich, G.K. and Peck, J.A., 2002. Muted climate variations in continental Siberia during the mid-Pleistocene epoch. Nature 418: 65–68.

Pross, J., Koutsodendris, A., Christanis, K., Fischer, T., Fletcher, W.J., Hardiman, M., Kalaitzidis, S., Knipping, M., Kotthoff, U., Milner, A.M., Müller, U.C., Schmiedl, G., Siavalas, G., Tzedakis, P.C. and Wulf, S., 2015. The 1.35-Ma-long terrestrial climate archive of Tenaghi Philippon, northeastern Greece: evolution, exploration, and perspectives for future research. Newsl. Stratigr. 48: 253–276.

Qiang, X.K., An, Z.S., Song, Y.G., Chang, H., Sun, Y.B., Liu, W.G., Ao, H., Dong, J.B., Fu, C.F., Wu, F., Lu, F.Y., Cai, Y.J., Zhou, W.J., Cao, J.J., Xu, X.W., Ai, L., 2011. New eolian red clay sequence on the western Chinese Loess Plateau linked to onset of Asian desertification about 25 Ma ago. Sci. China 54: 136–144.

Ravon, A.L., 2018. Land use in Brittany during the Middle Pleistocene: the example of the persistent place of Menez-Dregan I (Plouhinec, Finistère). In: Pope, M., McNabb, J. and Gamble, C.B.

(Editors), Crossing the Human Threshold: Dynamic Transformation and Persistent Places during the Middle Pleistocene. Routledge, London, pp. 106–122.

Ravon, A.L., Gaillard, C. and Monnier, J.L., 2016. Menez-Dregan (Plouhinec, Far Western Europe): the lithic industry from layer 7 and its Acheulian components. Quat. Int. 411: 132–143.

Raymo, M.E. and Mitrovica, J.X., 2012. Collapse of polar ice sheets during the stage 11 interglacial. Nature 483: 453–456.

Raymo, M.E., Oppo, D.W. and Curry, W., 1997. The mid-Pleistocene climate transition: a deep sea carbon isotopic perspective. Paleoceanography 12: 546–559.

Reich, D., Green, R.E., Kircher, M., Krause, J., Patterson, N., Durand, E.Y., Viola, B., Briggs, A.W., Stenzel, U., Johnson, P.L.F., Maricic, T., Good, J.M., Marques-Bonet, T., Alkan, C., Fu, Q.M., Mallick, S., Li, H., Meyer, M., Eichler, E.E., Stoneking, M., Richards, M., Talamo, S., Shunkov, M.V., Derevianko, A.P., Hublin, J.J., Kelso, J., Slatkin, M. and Pääbo, S., 2010. Genetic history of an archaic hominin group from Denisova Cave in Siberia. Nature 468: 1053–1060.

Ren, H.J., Sigman, D.M., Martínez-García, A., Anderson, R.F., Chen, M.T., Ravelo, A.C., Straub, M., Wong, G.T.F. and Haug, G.H., 2017. Impact of glacial/interglacial sea level change on the ocean nitrogen cycle. Proc. Natl. Acad. Sci. U. S. A. 114: E6759–E6766.

Reyes, A.V., Carlson, A.E., Beard, B.L., Hatfield, R.G., Stoner, J.S., Winsor, K., Welke, B. and Ullman, D.J., 2014. South Greenland ice-sheet collapse during Marine Isotope Stage 11. Nature 510: 525–528.

Richter, D., Grün, R., Joannes-Boyau, R., Steele, T.E., Amani, F., Rue, M., Fernandes, P., Raynal, J.P., Geraads, D., Ben-Ncer, A., Hublin, J.J. and McPherron, S.P., 2017. The age of the hominin

fossils from Jebel Irhoud, Morocco, and the origins of the Middle Stone Age. Nature 546: 293–296.

Rightmire, G.P., 1998. Human evolution in the Middle Pleistocene: the role of *Homo heidelbergensis*. Evol. Anthropol. 6: 218–227.

Rightmire, G.P., 2009. Middle and later Pleistocene hominins in Africa and Southwest Asia. Proc. Natl. Acad. Sci. U. S. A. 106: 16046–16050.

Rizal, Y., Westaway, K.E., Zaim, Y., van den Bergh, G.D., Bettis III, E.A., Morwood, M.J., Huffman, O.F., Grün, R., Joannes-Boyau, R., Bailey, R.M., Sidarto, Westaway, M.C., Kurniawan, I., Moore, M.W., Storey, M., Aziz, F., Suminto, Zhao, J.X., Aswan, Sipola, M.E., Larick, R.R., Zonneveld, J.-P., Scott, R., Putt, S. and Ciochon, R.L., 2019. Last appearance of *Homo erectus* at Ngandong, Java, 117,000–108,000 years ago. Nature 577: 381–385.

Roberts, M.B. and Parfitt, S.A., 1999. Boxgrove. A Middle Pleistocene hominid site at Eartham Quarry, Boxgrove, West Sussex. English Heritage, London.

Roebroeks, W. and Villa, P., 2011. On the earliest evidence for habitual use of fire in Europe. Proc. Natl. Acad. Sci. U. S. A. 108: 5209–5214.

Rohling, E.J., Grant, K., Bolshaw, M., Roberts, A.P., Siddall, M., Hemleben, C., Kucera, M., 2009. Antarctic temperature and global sea level closely coupled over the past five glacial cycles. Nat. Geosci. 2: 500–504.

Rohling, E.J., Foster, G.L., Grant, K.M., Marino, G., Roberts, A.P., Tamisiea, M.E. and Williams, F., 2014. Sea-level and deep-sea-temperature variability over the past 5.3 million years. Nature 508: 477–482.

Rosas, A., Bastir, M. and Alarcon, J.A., 2019. Tempo and mode in the Neandertal evolutionary lineage:

a structuralist approach to mandible variation. Quat. Sci. Rev. 217: 62–75.

Rossignol-Strick, M., Paterne, M., Bassinot, F.C., Emeis, K.C. and De Lange, G.J., 1998. An unusual mid-Pleistocene monsoon period over Africa and Asia. Nature 392: 269–272.

Schneider, T., Bischoff, T. and Haug, G.H., 2014. Migrations and dynamics of the intertropical convergence zone. Nature 513: 45–53.

Schoch, W.H., Bigga, G., Böhner, U., Richter, P. and Terberger, T., 2015. New insights on the wooden weapons from the Paleolithic site of Schöningen. J. Hum. Evol. 89: 214–225.

Scott, B. and Shaw, A.D., 2018. La Cotte de St Brelade Placemaking, assemblage and persistence in the Normano-Breton Gulf. In: Pope, M., McNabb J. and Gamble, C.B. (Editors), Crossing the Human Threshold: Dynamic Transformation and Persistent Places during the Middle Pleistocene. Routledge, London, pp. 142–164.

Shyu, J.P., Chen, M.P., Shieh, Y.T. and Huang, C.K., 2001. A Pleistocene paleoceanographic record from the north slope of the Spratly Islands, southern South China Sea. Mar. Micropaleontol. 42: 61–93.

Snyder, J.A., Cherepanova, M.V. and Bryan, A., 2013. Dynamic diatom response to changing climate 0–1.2 Ma at Lake Elgygytgyn, Far East Russian Arctic. Clim. Past. 9: 1309–1319.

Sosdian, S.M., Rosenthal, Y. and Toggweiler, J.R., 2018. Deep Atlantic carbonate ion and $CaCO_3$ compensation during the ice ages. Paleoceanogr. Paleoclimatol. 33: 546–562.

Spratt, R.M. and Lisiecki, L.E., 2016. A Late Pleistocene sea level stack. Clim. Past 12: 1079–1092.

Stockhecke, M., Kwiecien, O., Vigliotti, L., Anselmetti, F.S., Beer, J., Cagatay, M.N., Channell, J.E.T., Kipfer, R., Lachner, J., Litt, T., Pickarski, N. and Sturm, M., 2014. Chronostratigraphy of the 600,000 year old continental record of Lake Van (Turkey). Quat. Sci. Rev. 104: 8–17.

Stringer, C., 2012a. The status of *Homo heidelbergensis* (Schoetensack 1908). Evol. Anthropol. 21: 101–107.

Stringer, C., 2012b. What makes a modern human. Nature 485: 33–35.

Sun, Y.B., Clemens, S.C., An, Z.S. and Yu, Z.W., 2006. Astronomical timescale and palaeoclimatic implication of stacked 3.6-Myr monsoon records from the Chinese Loess Plateau. Quat. Sci. Rev. 25: 33–48.

Sun, Y.B., Yan, Y., Nie, J.S., Li, G.J., Shi, Z.G., Qiang, X.K., Chang, H., An, Z.S., 2020. Source-to-sink fluctuations of Asian eolian deposits since the late Oligocene. Earth-Sci. Rev. 200: 102963.

Shi, F., Yin, Q.Z., Nikolova, I., Berger, A., Ramstein, G., Guo, Z.T., 2020. Impacts of extremely asymmetrical polar ice sheets on the East Asian summer monsoon during the MIS-13 interglacial. Quat. Sci. Rev. 230: doi: 10.1016/j.quascirev.2020.106164.

Shiau, L.J., Yu, P.S., Wei, K.Y., Yamamoto, M., Lee, T.Q., Yu, E.F., Fang, T.H. and Chen, M.T., 2008. Sea surface temperature, productivity, and terrestrial flux variations of the southeastern South China Sea over the past 800 000 years (IMAGES MD972142). Terr. Atmos. Ocean. Sci. 19: 363–376.

Tiedemann, R., Sarnthein, M. and Shackleton, N.J., 1994. Astronomic timescale for the Pliocene Atlantic δ^{18}O and dust flux records of Ocean Drilling Program Site 659. Paleoceanography 9: 619–638.

Torrent, J., Liu, Q.S., Bloemendal, J. and Barrón, V., 2007. Magnetic enhancement and iron oxides in the upper Luochuan loess-paleosol sequence, Chinese Loess Plateau. Soil Sci. Soc. Am. J. 71: 1570–1578.

Torres, V., Hooghiemstra, H., Lourens, L. and Tzedakis, P.C., 2013. Astronomical tuning of long pollen records reveals the dynamic history of montane biomes and lake levels in the tropical high Andes during the Quaternary. Quat. Sci. Rev. 63: 59–72.

Tzedakis, P.C., Hooghiemstra, H. and Pälike, H., 2006. The last 1.35 million years at Tenaghi Philippon: revised chronostratigraphy and long-term vegetation trends. Quat. Sci. Rev. 25: 3416–3430.

Tzedakis, P.C., Raynaud, D., McManus, J.F., Berger, A., Brovkin, V. and Kiefer, T., 2009. Interglacial diversity. Nat. Geosci. 2: 751–755.

van den Bergh, G.D., Kaifu, Y., Kurniawan, I., Kono, R.T., Brumm, A., Setiyabudi, E., Aziz, F. and Morwood, M.J., 2016. *Homo floresiensis*-like fossils from the early Middle Pleistocene of Flores. Nature 534: 245–248.

Venz, K.A. and Hodell, D.A., 2002. New evidence for changes in Plio-Pleistocene deep water circulation from Southern Ocean ODP Leg 177 Site 1090. Palaeogeogr. Palaeoclimatol. Palaeoecol. 182: 197–220.

Voormolen, B., 2008. Ancient hunters, modern butchers: Schöningen 13II - 4, a kill-butchery site dating from the northwest European Lower Palaeolithic, University of Leiden.

Wang, P.X., Tian, J., Cheng, X.R., Liu, C.L. and Xu, J., 2003. Carbon reservoir changes preceded major ice-sheet expansion at the mid-Brunhes event. Geology 31: 239–242.

Wang, P.X., Li, Q.Y., Tian, J., Jian, Z.M., Liu, C.L., Li, L. and Ma, W.T., 2014. Long-term cycles in the carbon reservoir of the Quaternary ocean: a perspective from the South China Sea. Natl. Sci. Rev. 1: 119–143.

Wang, P.X., Wang, B., Cheng, H., Fasullo, J., Guo, Z.T., Kiefer, T. and Liu, Z.Y., 2017. The global

monsoon across time scales: mechanisms and outstanding issues. Earth-Sci. Rev. 174: 84–121.

Wolff, E.W., Barbante, C., Becagli, S., Bigler, M., Boutron, C.F., Castellano, E., de Angelis, M., Federer, U., Fischer, H., Fundel, F., Hansson, M., Hutterli, M., Jonsell, U., Karlin, T., Kaufmann, P., Lambert, F., Littot, G.C., Mulvaney, R., Rothlisberger, R., Ruth, U., Severi, M., Siggaard-Andersen, M.L., Sime, L.C., Steffensen, J.P., Stocker, T.F., Traversi, R., Twarloh, B., Udisti, R., Wagenbach, D. and Wegner, A., 2010. Changes in environment over the last 800,000 years from chemical analysis of the EPICA Dome C ice core. Quat. Sci. Rev. 29: 285–295.

Yin, Q.Z., 2013. Insolation-induced mid-Brunhes transition in Southern Ocean ventilation and deep-ocean temperature. Nature 494: 222–225.

Yin, Q.Z. and Berger, A., 2010. Insolation and CO_2 contribution to the interglacial climate before and after the Mid-Brunhes Event. Nat. Geosci. 3: 243–246.

Yin, Q.Z. and Berger, A., 2012. Individual contribution of insolation and CO_2 to the interglacial climates of the past 800,000 years. Clim. Dyn. 38: 709–724.

Zhang, H.B., Griffiths, M.L., Chiang, J.C.H., Kong, W.W., Wu, S.T., Atwood, A., Huang, J.H., Cheng, H., Ning, Y.F., Xie, S.C., 2018. East Asian hydroclimate modulated by the position of the westerlies during Termination I. Science 362: 580–583.

Zhang, J., Li, J.J., Guo, B.H., Ma, Z.H., Li, X.M., Ye, X.Y., Yu, H., Liu, J., Yang, C., Zhang, S.D., Song, C.H., Hui, Z.C. and Peng, T.J., 2016. Magnetostratigraphic age and monsoonal evolution recorded by the thickest Quaternary loess deposit of the Lanzhou region, western Chinese Loess Plateau. Quat. Sci. Rev. 139: 17–29.

Zhang, W.G., Yu, L.Z., Lu, M., Zheng, X.M., Ji, J.F., Zhou, L.M. and Wang, X.Y., 2009. East Asian

summer monsoon intensity inferred from iron oxide mineralogy in the Xiashu Loess in southern China. Quat. Sci. Rev. 28: 345–353.

Zhao, Y.L., Colin, C., Liu, Z.F., Paterne, M., Siani, G. and Xie, X., 2012. Reconstructing precipitation changes in northeastern Africa during the Quaternary by clay mineralogical and geochemical investigations of Nile deep-sea fan sediments. Quat. Sci. Rev. 57: 58–70.

Zheng, H.B., Wyrwoll, K.H., Li, Z.X. and Powell, C.M., 1998. Onset of aridity in southern Western Australia – a preliminary appraisal. Global Planet. Change 18: 175–187.

Zhou, L.P., Oldfield, F., Wintle, A.G., Robinson, S.G. and Wang, J.T., 1990. Partly pedogenic origin of magnetic variations in Chinese loess. Nature 346: 737–739.

Zhu, R.X., Hoffman, K.A., Potts, R., Deng, C.L., Pan, Y.X., Guo, B., Shi, C.D., Guo, Z.T., Yuan, B.Y., Hou, Y.M., Huang, W.W., 2001. Earliest presence of humans in northeast Asia. Nature 413: 413–417.

Zhu, R.X., An, Z.S., Potts, R., Hoffman, K.A., 2003. Magnetostratigraphic dating of early humans in China. Earth-Sci. Rev. 61: 341–359.

Zhu, R.X., Potts, R., Xie, F., Hoffman, K.A., Deng, C.L., Shi, C.D., Pan, Y.X., Wang, H.Q., Shi, R.P., Wang, Y.C., Shi, G.H., Wu, N.Q., 2004. New evidence on the earliest human presence at high northern latitudes in northeast Asia. Nature 431: 559–562.

Zhu, R.X., Potts, R., Pan, Y.X., Yao, H.T., Lu, L.Q., Zhao, X., Gao, X., Chen, L.W., Gao, F., Deng, C.L., 2008. Early evidence of the genus *Homo* in East Asia. J. Hum. Evol. 55: 1075–1085.

Zhu, Z.Y., Dennell, R., Huang, W.W., Wu, Y., Rao, Z.G., Qiu, S.F., Xie, J.B., Liu, W., Fu, S.Q., Han, J.W., Zhou, H.Y., Yang, T.P.O., Li, H.M., 2015. New dating of the *Homo erectus* cranium from Lantian (Gongwangling), China. J. Hum. Evol. 78: 144–157.

Zhu, Z.Y., Dennell, R., Huang, W.W., Wu, Y., Qiu, S.F., Yang, S.X., Rao, Z.G., Hou, Y.M., Xie, J.B., Han, J.W. and Ouyang, T.P., 2018. Hominin occupation of the Chinese Loess Plateau since about 2.1 million years ago. Nature 559: 608–612.

Ziegler, M., Lourens, L.J., Tuenter, E. and Reichart, G.J., 2010. High Arabian Sea productivity conditions during MIS 13-odd monsoon event or intensified overturning circulation at the end of the Mid-Pleistocene transition? Clim. Past 6: 63–76.

Figure captions

Figure 1. Boreal summer and winter patterns of precipitation and surface winds worldwide. High precipitation and convergence of surface winds (850 hPa) generally occurs at the ITCZ. Precipitation and wind data are from the Climate Prediction Centre Merged Analysis of Precipitation and from the European Centre for Medium Range Weather Forecasts (ECMWF) interim reanalysis between 1980 and 2005, respectively. Red and black solid circles represent sites that shifted to wetter and drier conditions from MIS 15 to 13, respectively. Red and black stars represent sites that shifted to more-warmed and less-warmed interglacial conditions from MIS 15 to 13, respectively.

Figure 2. Site location map and field photograph. (**A**) Map of the Chinese Loess Plateau (region with red solid dots) with mean annual precipitation contours (black dashed lines, numbers indicate annual rainfall in mm) and location of loess records discussed in the text (black solid circles), including Binxian, Luochuan, Jingchuan, Yimaguan, Sanmenxia, Duanjiapo, Xifeng, Lingtai, and Xijin. The Yellow River is the major river system in North China. (**B**) Field photograph of the Binxian

loess sequence. L and S indicates loess and palaeosol layers, respectively.

Figure 3. Comparison of various loess χ_{lf} time scales and age model construction for the Binxian loess section. (**A**) Binxian lithology and χ_{lf} plotted against depth. (**B**) Comparison between Binxian and Xifeng χ_{lf} records on the age model of Guo et al. (2009) established by loess-to-marine correlations. (**C**) Comparison of the established Binxian χ_{lf} time series with the LR04 marine benthic $\delta^{18}O$ stack (Lisiecki and Raymo, 2005). (**D–F**) Astronomical time scales for the Jingchuan (Ding et al., 2002), Lingtai (Sun et al., 2006), and Luochuan (Heslop et al. 2000) loess χ_{lf} records. (**G**) Yimaguan loess χ_{lf} placed on a time scale (Hao et al., 2012) established by a combination of loess-to-marine correlations and a weighted grain-size age model proposed by Porter and An (1995). Black dots on the Binxian χ_{lf} record represent tie points used to establish the age model. Blue bars indicate the correlation of thick marker palaeosol (S_5 and S_4) layers to interglacial stages.

Figure 4. Chinese loess Asian summer monsoon proxies over the past 800 kyr. (**A–J**) East Asian summer monsoon precipitation variability on the Chinese Loess Plateau indicated by loess χ_{fd} from the Luochuan section (Hao et al., 2012) and Xijing core (Zhang et al., 2016), and by χ_{lf} from loess sections at Luochuan (Hao et al., 2012), Lingtian (Sun et al., 2006), Jingchuan (Ding et al., 2002), Yimaguan (Hao et al., 2012), Sanmenxia (Li et al., 2017b), Duanjiapo (An et al., 2005), Xifeng (Sun et al., 2006), and Binxian (this study). All loess proxy records refer to the age model of Guo et al. (2009). (**K**) LR04 benthic $\delta^{18}O$ stack (Lisiecki and Raymo, 2005). Temporal χ_{lf} and χ_{fd} variability during the last 800 kyr is similar across the Chinese Loess Plateau, with all records suggesting prominently higher interglacial East Asian summer monsoon precipitation from MIS 13 onward.

53

Glacial-interglacial cycles are clearly evident in all records, although details differ slightly in different records, which is consistent with their respective resolutions and regionally variable pedogenic development related to monsoon palaeoprecipitation variations.

Figure 5. Monsoon precipitation, global ocean carbon chemistry, and global climate variability over the past 800 kyr. (A, B) East Asian summer monsoon precipitation variability on the Chinese Loess Plateau indicated by the Binxian (BX) loess χ_{lf} and Hm/Gt records (this study). **(C)** South Asian monsoon precipitation indicated by the Arabian Sea Ca/K record (Kunkelova et al., 2018). **(D)** North African monsoon precipitation variability inferred from the clay-mineralogical illite-chemistry index (ratio of the 5 Å and 10 Å peak areas, which correlates positively with precipitation) of Nile deep-sea fan sediments in the Levantine Basin (Zhao et al., 2012). **(E)** Amazon precipitation inferred from $CaCO_3$ concentration at Ceara Rise (Harris et al., 1997). **(F)** South African monsoon precipitation variability inferred from ln(Fe/Ca) ratios in marine core MD96-2048, offshore southeastern Africa (Caley et al., 2018). **(G)** Ocean carbon chemistry variability inferred from a benthic $\delta^{13}C$ stack from ODP Sites 1143, 849, 659, 1123, and 1090 $\delta^{13}C$ records (see Fig. 8 for details). **(H)** Atmospheric CO_2 concentration reconstructed from the Antarctic Dome C ice core (Lüthi et al., 2008). **(I)** Global mean annual surface air temperature (ΔMAT) changes (Martínez-Botí et al., 2015). **(J)** ODP Site 1123 (South Pacific Ocean) deep-sea temperature (5-point running average of original data) based on Mg/Ca ratios from benthic foraminifera (Elderfield et al., 2012). **(K)** Global sea level (Spratt and Lisiecki, 2016). **(L)** LR04 benthic $\delta^{18}O$ stack (Lisiecki and Raymo, 2005). The first stage (MBT-1) was associated with monsoon precipitation and carbon reservoir changes during MIS 13, while the second stage (MBT-2) was marked by global temperature and ice volume/sea level shifts during MIS

11, which were linked to increased atmospheric CO_2 concentrations.

Figure 6. Hydroclimate variability in South Asia and the tropical Pacific Ocean over the past 800 kyr. (A) Precipitation variability in South Asia inferred from X-ray fluorescence (XRF) scanning Ba counts of marine sediment core MD04-2881 from the Arabian Sea (Ziegler et al., 2010). **(B–D)** Precipitation variability in the tropical Pacific Ocean inferred from ODP Hole 806B planktonic foraminiferal (*Globigerinoides ruber*) $\delta^{18}O$ and seawater $\delta^{18}O$ records (Medina-Elizalde and Lea, 2005), and core PC72 sedimentary biogenic opal flux (Murray et al., 2012). **(E)** LR04 benthic $\delta^{18}O$ stack (Lisiecki and Raymo, 2005). MIS 13 has higher precipitation in South Asia and tropical Pacific Ocean than previous interglacials.

Figure 7. High-latitude northern hemisphere continental and southern hemisphere climate variability across the MBT. (A) δD temperature from the Antarctic Dome C ice core (Jouzel et al., 2007). **(B, C)** Alkenone-based SST records from ODP Sites 1090 and 1082, South Atlantic Ocean (Etourneau et al., 2009; Martinez-Garcia et al., 2009). **(D)** SST record based on tetraether index (TEX_{86}) from core MD96-2048, offshore southeastern Africa (Caley et al., 2011). **(E)** Southern hemisphere SST stack based on the ODP Sites 1082 and 1090 and core MD96-2048 records. **(F)** Sea-salt sodium flux from the Antarctic Dome C ice core (Wolff et al., 2010) (note the inverse axis). Higher sodium flux reflects larger Antarctic ice extents. **(G)** Simulated West Antarctic ice sheet variability (Pollard and Deconto, 2009). **(H)** XRF scanning Mn content in piston core 92AR-P39, western Arctic Ocean (Polyak et al., 2013). High-Mn units represent interglacial interstadial intervals, which are linked to higher continental margin input due to lower Arctic sea-ice extent. **(I, J)**

Abundance of spermatophyte and pteridophyte pollen at ODP Site 646, Labrador Sea (de Vernal and Hillaire-Marcel, 2008). **(K, L)** Mn/Fe and diatom concentrations at Lake El'gygytgyn, NE Russia (Melles et al., 2012; Snyder et al., 2013). Lower southern than northern hemisphere continent interglacial warming displaced the ITCZ northward from MIS 15 to 13 and caused monsoon precipitation and carbon reservoir changes during MBT-1 at 500 ka.

Figure 8. Comparison of Ocean carbon chemistry variability with benthic δ^{18}O over the past 800 kyr. (A–E) Ocean carbon chemistry variability inferred from benthic δ^{13}C records from ODP Sites 1143 (South China Sea) (Wang et al., 2003), 849 (tropical eastern Pacific Ocean) (Mix et al., 1995), 659 (North Atlantic Ocean) (Tiedemann et al., 1994), 1123 (South Pacific Ocean) (Elderfield et al., 2012), and 1090 (Southern Ocean) (Venz and Hodel, 2002). **(F)** Stacked benthic δ^{13}C based on ODP Sites 1143, 849, 659, 1123, and 1090. **(G)** LR04 benthic δ^{18}O stack (Lisiecki and Raymo, 2005). Maximum positive benthic δ^{13}C values during MIS 13 suggest carbon reservoir changes.

Figure 9. Deep-water circulation (DWC) variability over the past 800 kyr. (A–B) DWC variability inferred from ODP Site 929 seawater ε_{Nd}, equatorial western Atlantic Ocean (Howe and Piotrowski, 2017), benthic foraminiferal trace element B/Ca record compiled from DSDP Site 607 and a nearby piston core, North Atlantic Ocean (Sosdian et al., 2018), and South Atlantic Core GeoB 3813-3 kaolinite/chlorite (Gingele and Schmieder, 2001). **(C)** LR04 benthic δ^{18}O stack (Lisiecki and Raymo, 2005). The onset of unusually high interglacial Asian summer monsoon precipitation (Fig. 4) and carbon reservoir changes (Fig. 8) occurred during MIS 13, during which deep-water circulation did not change markedly during MIS 13 when benthic δ^{13}C has maximum positive values relative to previous interglacials.

Figure 10. Global climatic variability and development of mid-Pleistocene hominins and technology over the last 800,000 years. Increased global climate variability across the MBT inferred from the LR04 benthic δ^{18}O stack (Lisiecki and Raymo, 2005) is correlated with increased hominin diversity and (in many regions) Levallois development from handaxe technology. Inferred age ranges of hominin lineages are shown, with colours reflecting commonly accepted species designations (Galway-Witham et al., 2019). Dotted lines indicate possible phylogenetic associations of lineages.

Table 1

Palaeoclimate records used to document the shift to higher precipitation in Asia, North Africa, Europe, northern South America, and the equatorial Pacific Ocean, and to lower precipitation in South Africa and Australia during MIS 13. The respective site locations are indicated in Figure 1.

Regions	Sites	Records	Proxies	References
Asia	Chinese Loess Plateau, central China	Loess	χ_{lf}; χ_{fd}; Hm/Gt; Fe_d/Fe_t	This study; Ding et al. (2002); An et al. (2005); Sun et al. (2006); Guo et al. (2009); Hao et al. (2012); Zhang et al. (2016); Li et al. (2017b); Lu et al. (2020)
	Yinchuan Basin, northwest China	Fluvial-lacustrine	Pollen	Li et al. (2017a)
	South China	Loess and soil	Soil micromorphology; chemical weathering proxies; environmental magnetic proxies	Zhang et al. (2009); Lu et al. (2020)
	South China Sea	Marine	n-alkane flux; sea-surface salinity; $\delta^{15}N$; opal content	Shyu et al. (2001); Shiau et al. (2008); Li et al. (2013); Ren et al. (2017)
	Arabian Sea	Marine	Ca/K; Ba concentration; grain size	Clemens et al. (1996); Ziegler et al. (2010)
North Africa	Mediterranean Sea	Marine	Sapropel development, Si/Al; K/Al; clay mineralogy	Rossignol-Strick et al. (1998); Zhao et al. (2012)
	Sahara Desert	Fluvial-lacustrine and aeolian	Ephemeral lake growth	Geyh and Thiedig (2008)
Middle East	Lake Van	Lacustrine	Pollen; TOC; Ca/K	Litt et al. (2014); Stockhecke et al. (2014)
Europe	Danube River basin	Loess	χ_{lf}	Marković et al. (2015)
Northernmost South America	Ceara Rise	Marine	$CaCO_3$ concentration	Harris et al. (1997)
	Northern Colombia	Lacustrine	Pollen	Hooghiemstra and Ran (1994); Torres et al. (2013)
Equatorial Pacific Ocean	ODP Hole 806B	Marine	*Globigerinoides ruber* $\delta^{18}O$; seawater $\delta^{18}O$	Medina-Elizalde and Lea (2005);
	Core HY04	Marine	n-alkane $C_{31}/(C_{29} + C_{31})$	Horikawa et al. (2010)
	Core PC72	Marine	Opal flux	Murray et al. (2012)
South Africa	Core MD96-2048	Marine	Fe/Ca	Caley et al. (2018);
	Lake Magadi	Lacustrine	Pollen	Owen et al. (2018)
Australia	Lake Bungunnia	Lacustrine	Sedimentology	An et al. (1986)
	Lake Lefroy	Lacustrine	Sedimentology	Zheng et al. (1998)

Table 2

Palaeoclimate records used to document less-warmed southern hemisphere and more-warmed northern hemisphere continents during MIS 13. The respective site locations are indicated in Figure 1.

Regions	Sites	Records	Proxies	References
Southern hemisphere	ODP Site 1123, sub-Antarctic Pacific Ocean	Marine	Mg/Ca deep-sea temperature	Elderfield et al. (2012)
	Antarctic	Ice core	δD temperature; sea-salt sodium flux	Jouzel et al. (2007); Wolff et al. (2010)
	ODP Sites 1090 and 1082, South Atlantic Ocean	Marine	Alkenone-based SST	Etourneau et al. (2009); Martínez-Garcia et al. (2009)
	Core MD96-2048, southeastern Africa	Marine	TEX_{86}-based SST	Caley et al. (2011)
	ODP Site 1094, South Atlantic Ocean	Marine	Ba/Fe; Ca/Fe	Jaccard et al. (2013)
Northern hemisphere	Arctic Ocean	Marine	Pollen	de Vernal and Hillaire-Marcel (2008); Polyak et al. (2013)
	New Mexico	Lacustrine	Pollen; temperature reconstruction	Fawcett et al. (2011); Contreras et al. (2016)
	Britain	Terrestrial	Palaeoecology	Candy and McClymont (2013)
	Zoige palaeolake, Eastern Tibetan Plateau	Lacustrine	Carbonate concentration; pollen	Chen et al. (1999)
	Tenaghi Phillipon, Greece	Lacustrine	Pollen	Pross et al. (2015)
	Italy	Terrestrial and marine	Pollen	Combourieu-Nebout et al. (2015); Margari et al. (2018)
	Lake Baikal	Lacustrine	Diatom	Prokopenko et al. (2002)
	Lake El'gygytgyn	Lacustrine	Mn/Fe; diatom	Melles et al. (2012); Snyder et al. (2013)

Declaration of interests

☒ The authors declare that they have no known competing financial interests or personal relationships that could have appeared to influence the work reported in this paper.
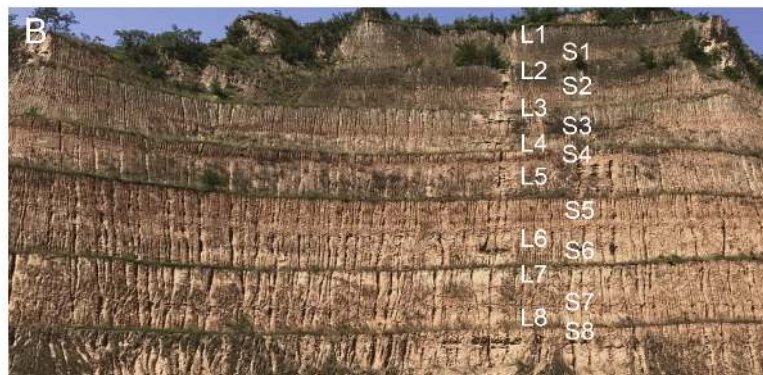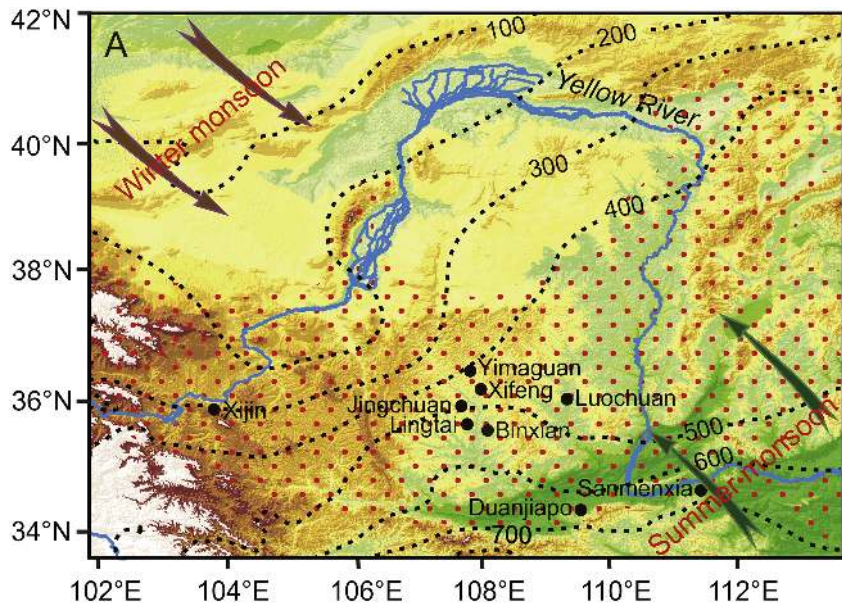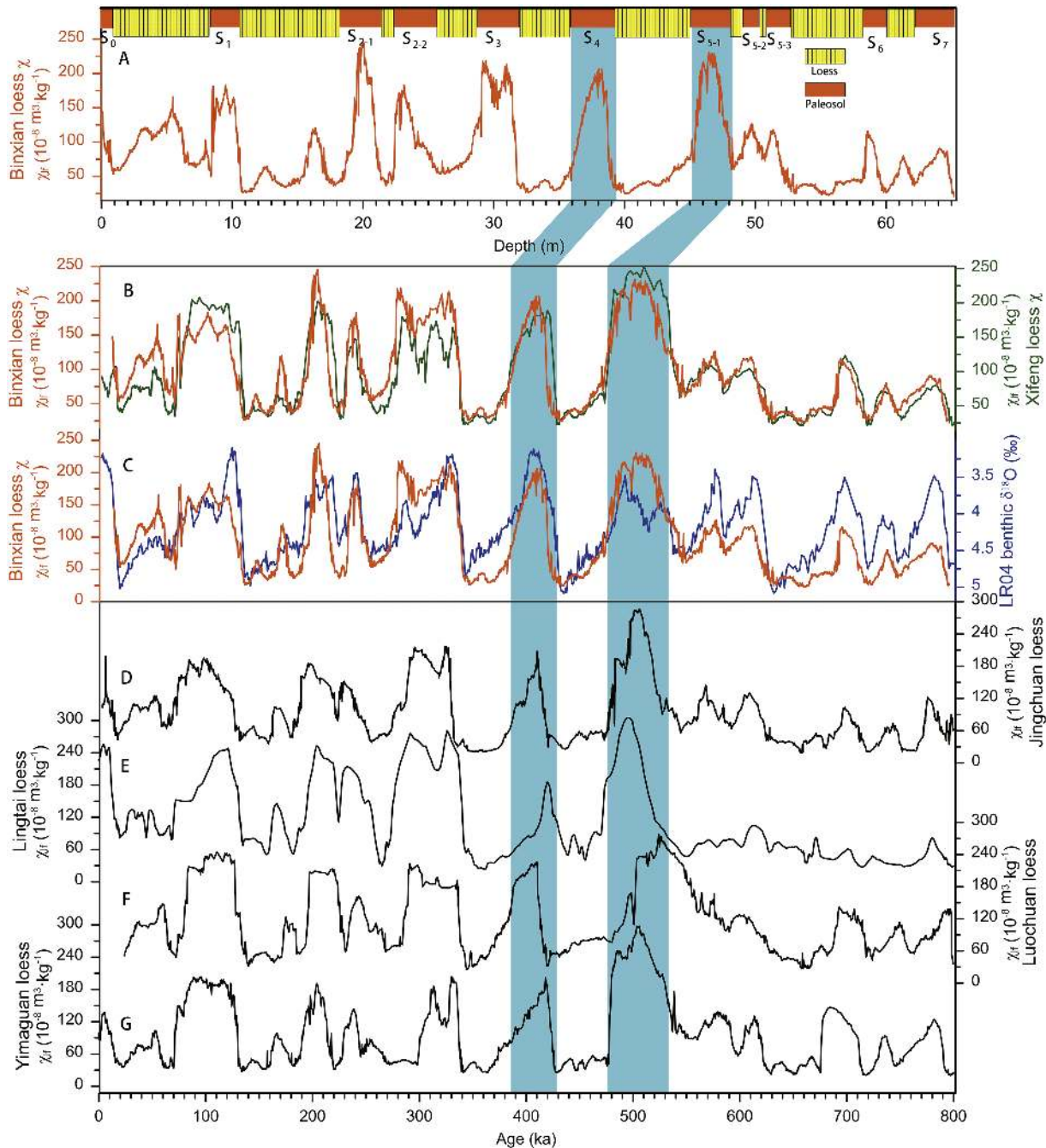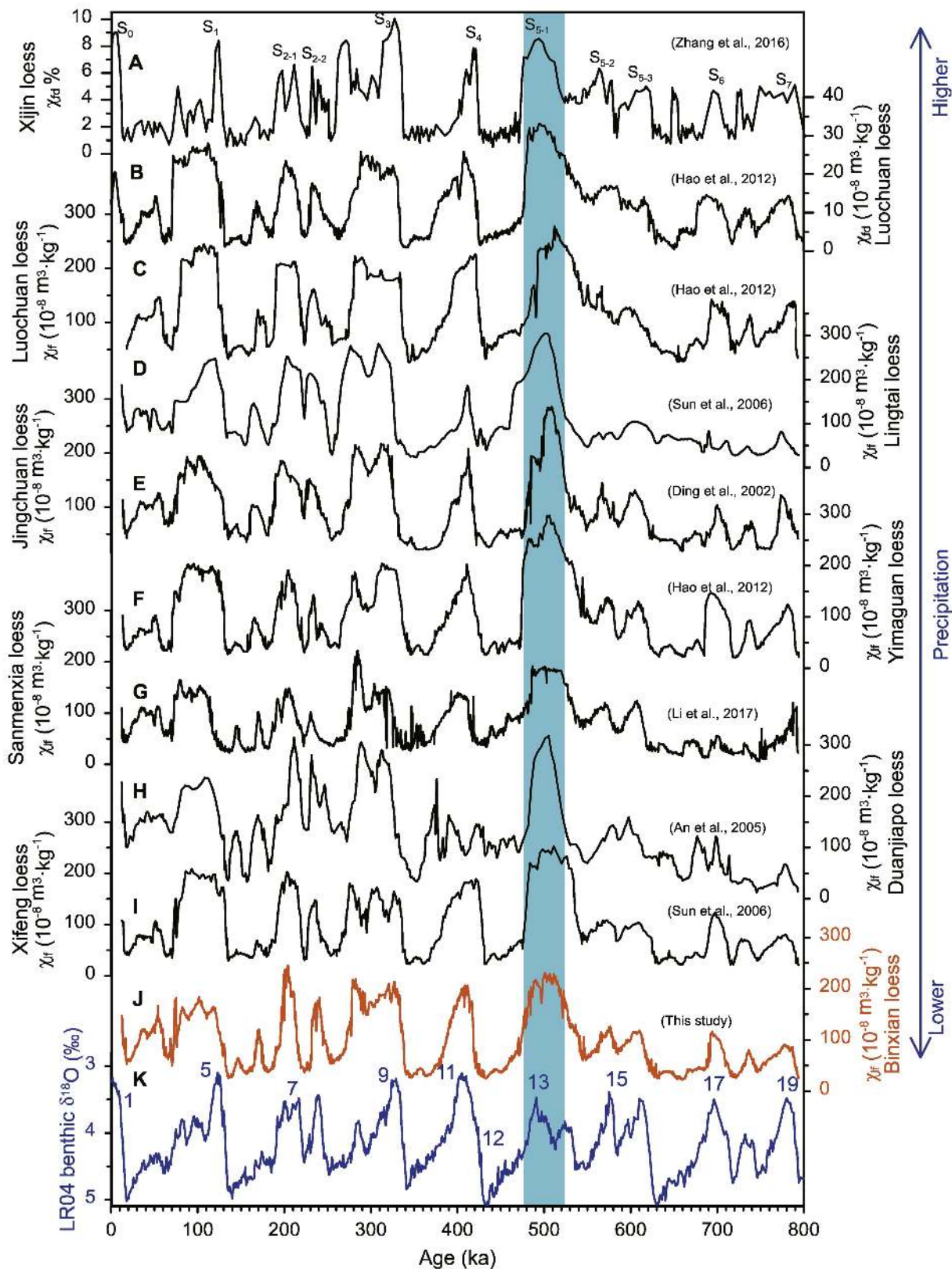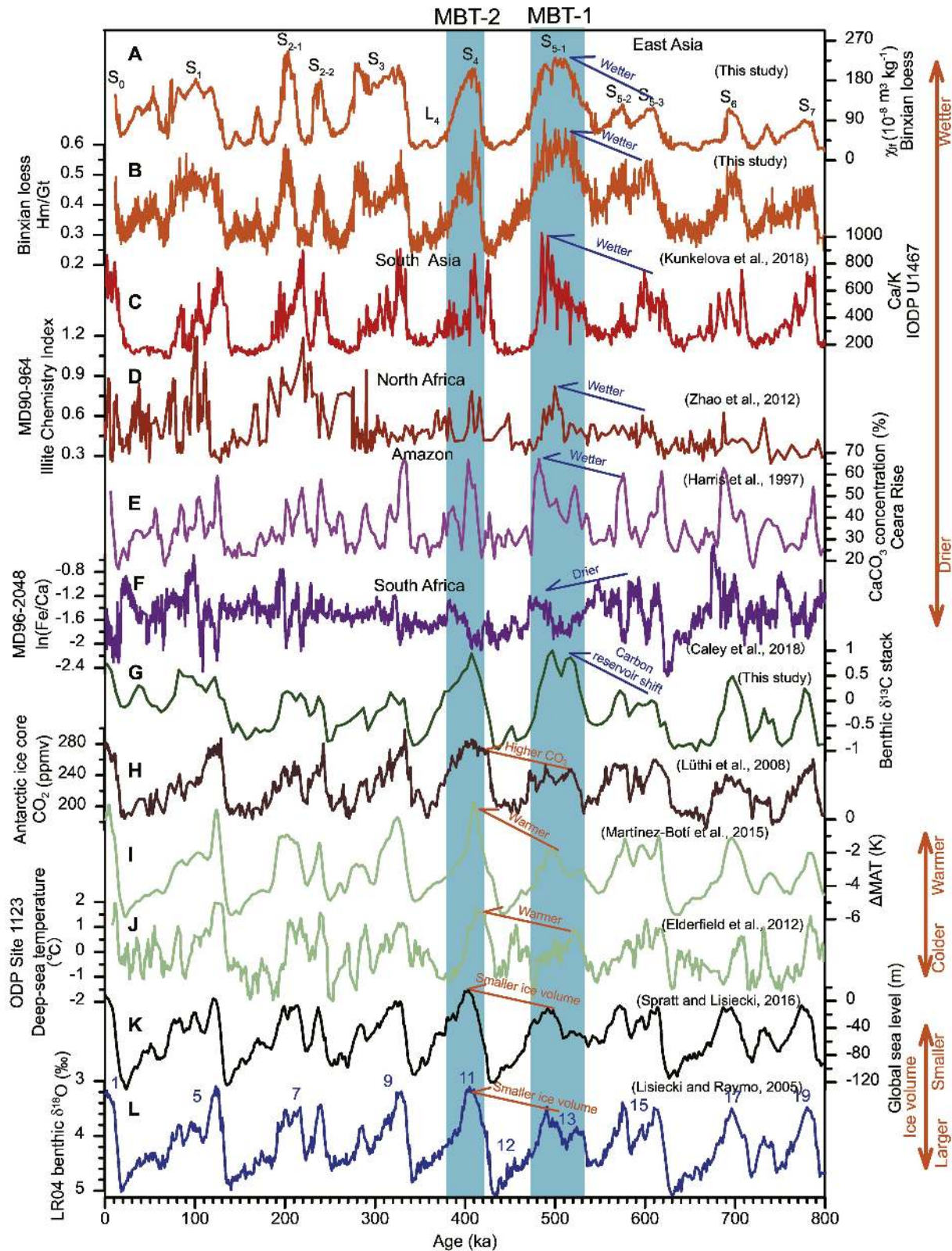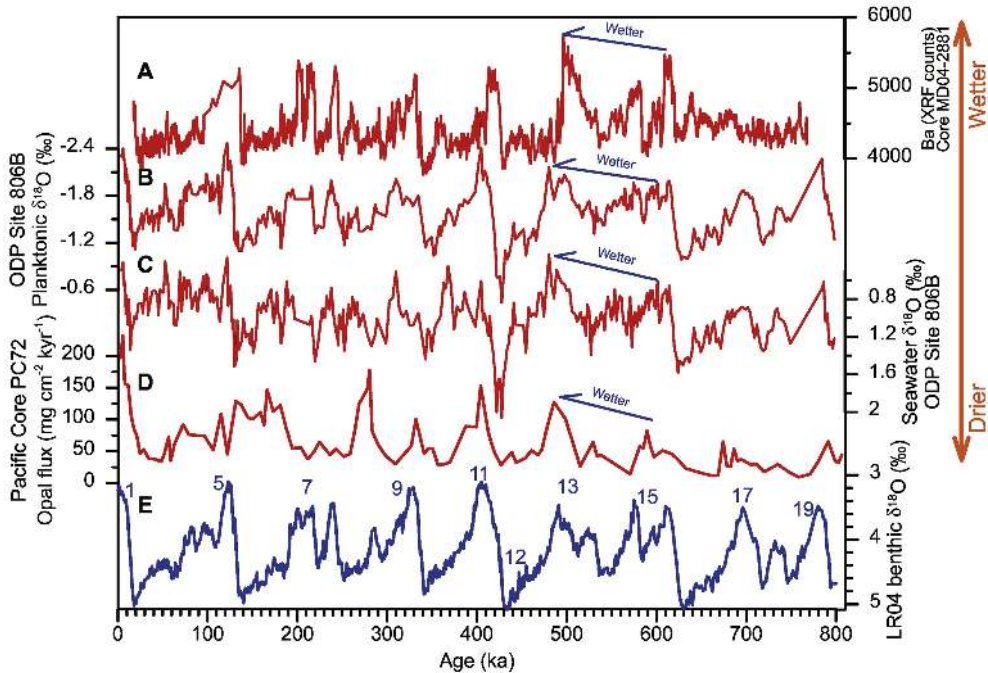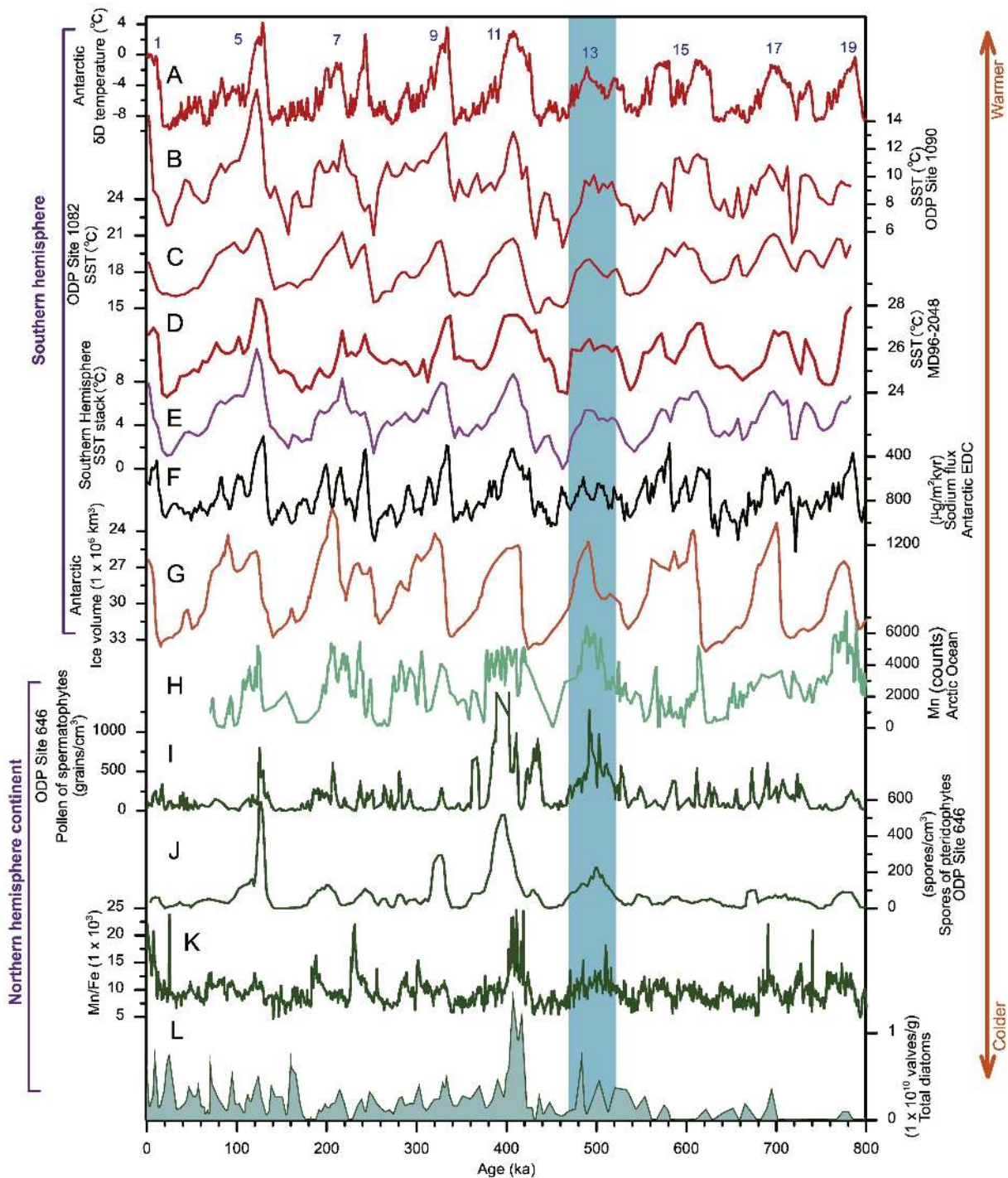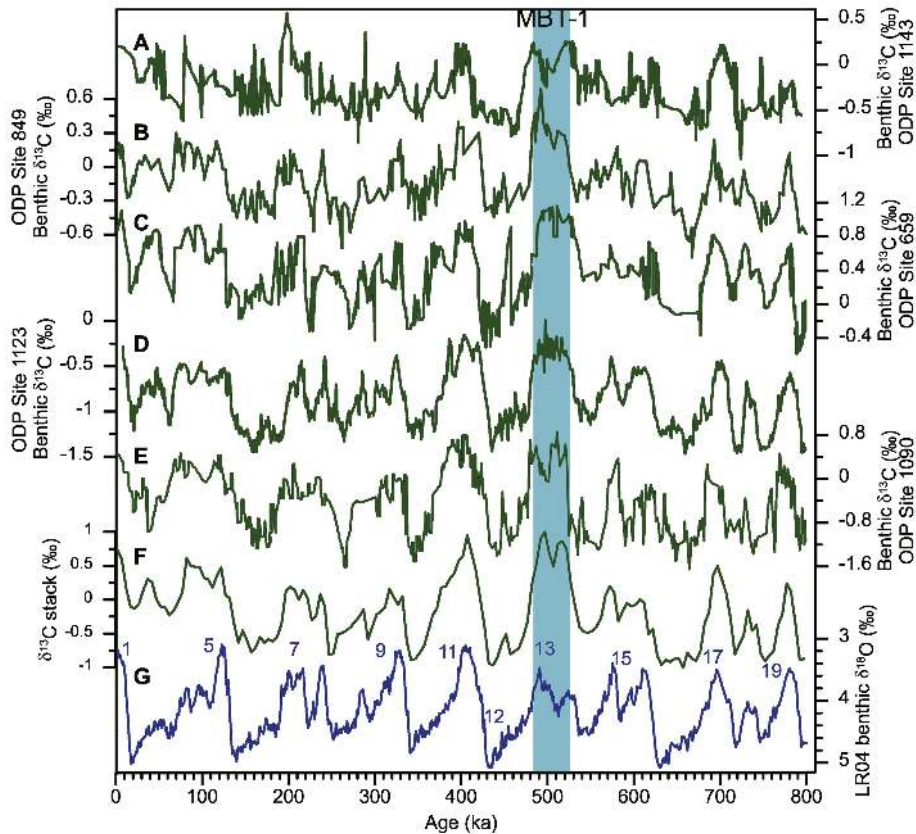
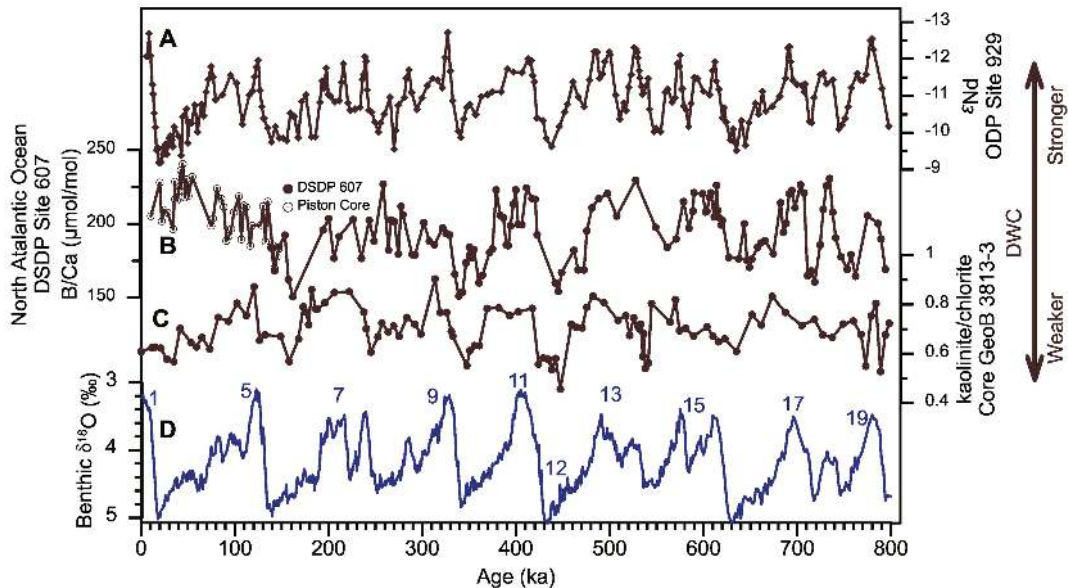Declaration of interests
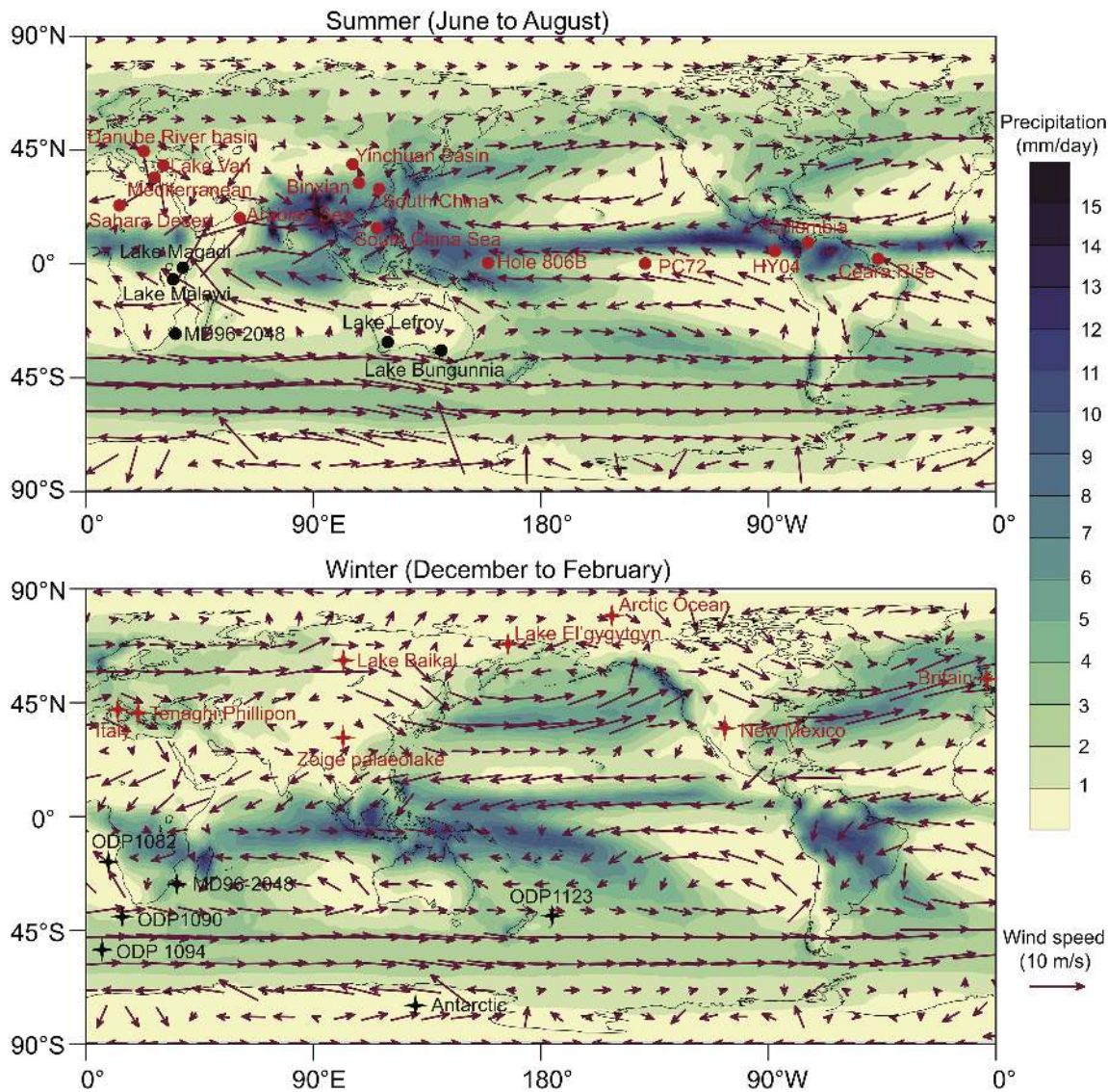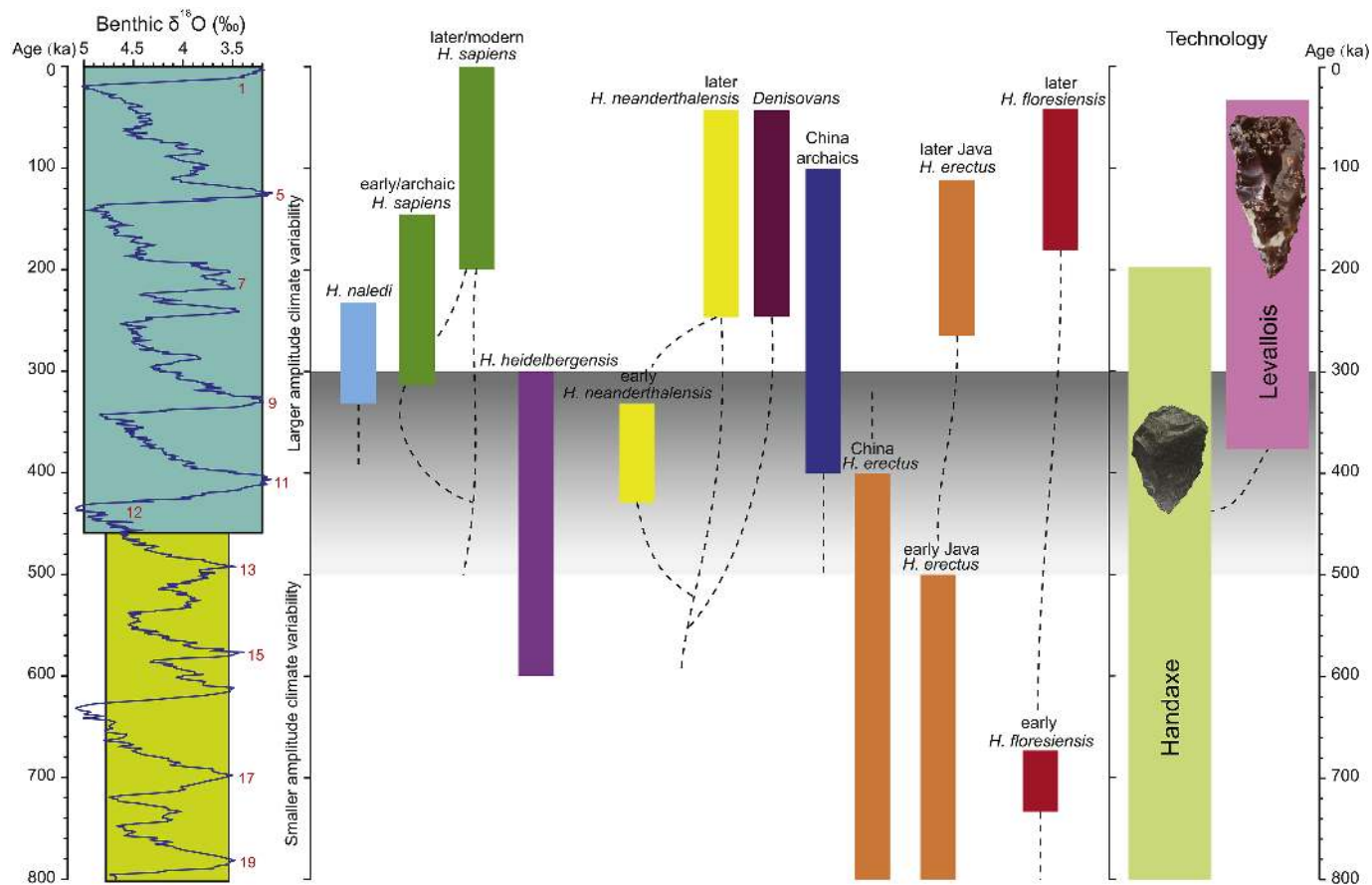
Figure 1

Figure 2

Figure 3

Figure 4

Figure 5

Figure 6

Figure 7

Figure 8

Figure 9

Figure 10